UNIVERSIDADE DE COIMBRA

Linearity Studies of the TileCal detector PMTs of ATLAS/LHC experiment, with the Laser monitoring system

by

Bruno Miguel Leonardo Galhardo

Dissertation submitted in partial fulfillment of the requirements for the Masters Degree in Nuclear Particles and Physics

in the

Faculdade de Ciências e Tecnologia da Universidade de Coimbra

Departamento de Física

Supervisor: Professor Doutor João Carlos Lopes Carvalho

July 2010

UNIVERSIDADE DE COIMBRA

Abstract

Faculdade de Ciências e Tecnologia da Universidade de Coimbra
Departamento de Física

Masters Degree in Nuclear Particles and Physics

by Bruno Miguel Leonardo Galhardo

An important parameter of the performance of a detector is its linear response. In TileCal, an hadron calorimeter of scintillating tiles, the light is transmitted by optical fibers wavelength shifting to be readout by photomultiplier tubes (PMT). They must have a response that increases linearly with the intensity of light received, which is proportional to the energy deposited by particles in the calorimeter. To measure the linearity of the PMT one uses a laser system that sends both a well-defined quantity of light, monitored by PMT and photodiodes installed inside the laser box, to all of the approximately 10 000 PMT in TileCal. In this study was developed software for data analysis, using the ROOT program, to study the linearity of the response of the PMTs.

UNIVERSIDADE DE COIMBRA

Abstract

Faculdade de Ciências e Tecnologia da Universidade de Coimbra
Departamento de Física

Masters Degree in Nuclear Particles and Physics

by Bruno Miguel Leonardo Galhardo

Um parâmetro importante para a medida do desempenho de um detector é a sua linearidade de resposta. No TileCal, um calorímetro hadrónico de telhas cintilantes, a luz de cintilação é transmitida por fibras ópticas, com mudança do comprimento de onda, para leitura por tubos fotomultiplicadores (PMT). Estes têm de ter uma resposta que aumenta linearmente com a intensidade de luz recebida, a qual será proporcional à energia depositada pelas partículas no calorímetro. Para medir a linearidade dos PMT recorre-se a um sistema laser que envia, simultaneamente, uma quantidade bem definida de luz, monitorizada por PMT e fotodíodos instalados dentro da caixa do laser, para todos os cerca de 10000 PMT do TileCal. Neste trabalho desenvolveu-se software de análise de dados, recorrendo ao programa ROOT, para o estudo da linearidade de resposta dos PMT.

Acknowledgements

First of all i would like to thank my supervisor, João Carvalho, for his outstanding guidance and dedication. I also want to thank my office colleagues and friends Susana e Inês for their availability in helping me.

A big thanks to Miguel, for his huge help and hospitality in Switzerland, without it, i would had a hard time adapting there.

I thank all my friends for for all the fun, fellowship and motivation especially Ângela for her true friendship, support and also some patience.

Finally i would like to thank my family for their continual and unconditional support and affection.

Contents

List of Figures

List of Tables

Chapter 1

Introduction

At present, all the observable phenomena can be explain by four fundamental interactions: the gravitation has a very weak intensity and acts on all matter; its importance is taken into account on large systems but is negligible in particle physics (its incorporation in particle physics remains a problem unsolved by theoretical physics). The electromagnetic interaction is responsible for the cohesion of the atoms and a large portion of the phenomena observable at our scale; the strong and weak interactions are responsible for the cohesion of the atomic nuclei and radioactivity, respectively. The ultimate goal of particle physics is to find a theory that explains and unifies all these interactions.

The Standard Model is a theory comprising: first, the electroweak theory (electromagnetic interaction and weak interaction) and, secondly, the strong interaction. To this day, all observed experimental particle physics phenomenon are explained by this theory. All the particles in this theory (3 families/generations of fermions with 2 quarks, a lepton and its neutrino, and 4 boson mediators) were found by experiments except one, the Higgs boson.

With the purpose of testing the Standard Model and eventually alternative models beyond the Standard Model, the Large Hadron Collider (LHC), was built at CERN (European Organization for Nuclear Research). It is a proton-proton collider and will reach a maximum energy of 14 TeV. In order to study the particle collisions, four detectors are placed on LHC. One of them is ATLAS (A Toroidal LHC ApparatuS) and its sub-detector TileCal is the one of interest in this work.

In order to provide the best possible physics input, the TileCal response must be perfectly understood and optimized, so that the difference between the energy of the particle and the energy we are reconstructing should be as small as possible. This is the role of the calibration.

One of 3 systems used to calibrate the hardware in TileCal is the LASER system. It is used to calibrate and monitor all 9852 photomultipliers tubes (along with their associated electronics) within the detector. The focus of this work will be an analysis of the linearity response of those TileCal PMTs using this LASER system.

This thesis is structured as follows. In the second chapter, the accelerator (LHC) and the ATLAS detector are presented. On the third chapter is described the calibration tools, in particular the LASER system used in TileCal. On the fourth chapter is presented the analysis and results of the linearity of the PMTs using the LASER system with runs having only one intensity at a time. On chapter five is shown the analysis and results, this time using different intensity runs. Lastly, chapter 6 is left for the conclusions and comments about this study.

Chapter 2

ATLAS Detector

2.1 LHC

With the purpose of studying the physics of particles under the framework of the Standard Model and other models beyond the Standard Model, the LHC was built. It is a proton-proton collider located at CERN, near Geneva, Switzerland. This accelerator will allow to access masses in the interval of a few GeV and several TeV. The motivation behind the construction of this machines are the following:

- Comprehension of the origin of masses of the particles: currently, the Standard Model explains this by the Higgs Mechanism which assumes a neutral boson called Higgs boson. This particle could have a mass of 120GeV or all the way to 1TeV.
- Physics beyond the Standard Model: although the Standard Model gives predictions verified to a level of 0.1%, some of its theoretical flaws (unification of coupling constants, number of families, ...) suggest that this model is an approximation, at low energy, of some more general model. So, the LHC will allow to observe manifestations of these eventual new theories until energies of order of a TeV.
- Answering some open questions such as: are quarks and leptons the elementary particles? What is the origin of the asymmetry between matter and anti-matter? What is the origin of confinement of quarks?
- Precision measurements (Top mass, W width): due to the high luminosity of LHC, measurements involving a large statistics can be made. They will test more thoroughly the predictions of the Standard Model.

The accelerator was built in the LEP (Large Electron Positron collider) tunnel and is 27km long and is placed 50-175m underground. The particles are accelerated by

intense electric fields. An intense magnetic field of 8.4T will maintain the trajectory of the protons in the ring. The acceleration of protons will be made in several stages of accelerations, in various accelerators, to achieve the nominal energy. This chain is represented in 2.1. The Linac2 will accelerate protons up to an energy of 50MeV. The Booster (PSB) will reach an energy of 1GeV. The protons will be sent to PS bringing their energy to 26GeV. Finally, the SPS will provide, as output, a beam of protons of 450GeV, which is injected into the LHC and where it reaches its nominal energy of 7TeV.

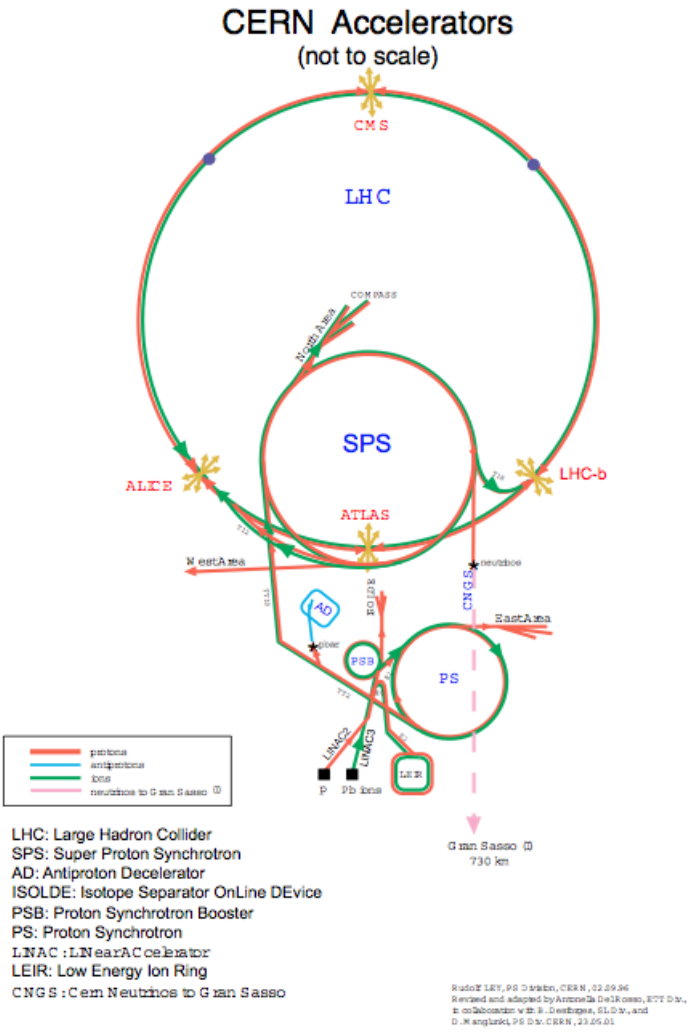

FIGURE 2.1: LHC acceleration stages

Four main experiments are installed at LHC: ATLAS and CMS (Compact Muon Solenoid) are generalist experiments aiming to discover the Higgs boson or evidences of supersymmetry among other things. Then there is ALICE (A Large Ion Collider Experiment) which is focused in the study of heavy ion collisions (Pb-Pb). Its researches will search

for evidence of a plasma of quarks and gluons. Lastly is LHCb which is dedicated to the study o the violation of CP symmetry.

2.2 ATLAS Detector

The ATLAS detector is constituted of a set of sub detectors of cylindrical shape placed around the beam pipe. The sub-detectors form layers around the collision point. In this way, the particles emitted transversely pass through three types of sub-detectors:

- The inner tracker: it measures charged particles tracks and their momentum. The curvature of the tracks is obtained thanks to the magnetic field of 2T produced by a magnetic solenoid. It allows the determination of primary and secondary vertices.
- The Calorimeters: two types of calorimeters are being used, the electromagnetic followed by the hadronic. The electromagnetic calorimeter was designed to measure the energy of charged particles and photons through the electromagnetic interaction, while the hadronic calorimeter measures the energy of hadrons that interact via the strong interaction.
- The muon spectrometer: identifies and measures the momentum of muons. The curvature of the trajectory of these particles is obtained by a toroid magnet.

Besides this, there are the two magnetic systems: a solenoid surrounding the Inner Detector and the toroid magnets. The toroid magnets surround the calorimeters and generate the magnetic field for the muon spectrometer.

One important variable used in ATLAS is the pseudo-rapidity, and is defined as

$$\eta = -ln(tan\left(\frac{\theta}{2}\right)) \tag{2.1}$$

Where θ is the polar angle (the azimuthal angle is ϕ). η is then related with the angle between the object momentum and the beam pipe (z-axis). Its variation with θ is plotted on Figure 2.2.

To achieve its goals, the detector needs to fulfill a set of requirements[1]:

- Fast electronics, resistant to the radiation, and high granularity to reduce events overlap.

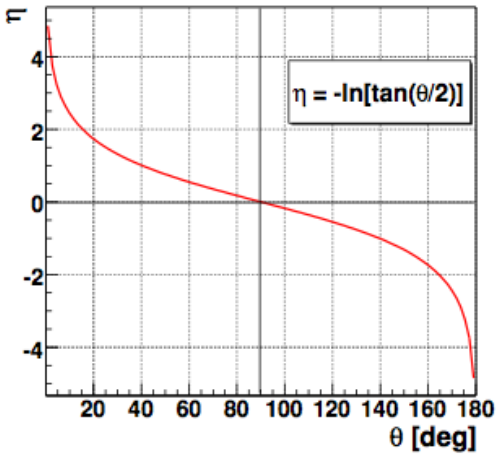

FIGURE 2.2: Pseudorapidity (η) as a function of the polar angle (θ).

- Large acceptance in pseudo-rapidity, with a very large coverage in the azimuthal angle.
- Good resolution in the charged particles momentum and reconstruction efficiency in the Inner Detector. Pixel detectors close to the interaction point are required for an efficient triggering and offline tagging of τ's and b-jets by observation of secondary vertices.
- An electromagnetic calorimeter with an excelent capability of identification and measurement of photons and electrons and an accurate hadronic calorimeter to measure jet and missing transverse energy with precision.
- An independent muon identification with good momentum resolution to determine unambiguously the charge of high p_T muons.
- A triggering system for low p_T particles with sufficient background rejection to allow the observation of most of the physics processes of interest at the LHC.

The structure of the detector is shown on Figure 2.3 and the general performance goals of ATLAS detector are on Table 2.1 [1]

2.2.1 Inner Detector

The inner detector determines the trajectories of the charged particles, their momentum and the primary and secondary vertices. It allows the identification of electrons, labeling of b-jets, τ leptons and the rejection of light jets. The objectives in terms of performance of the sub-detector are [2]:

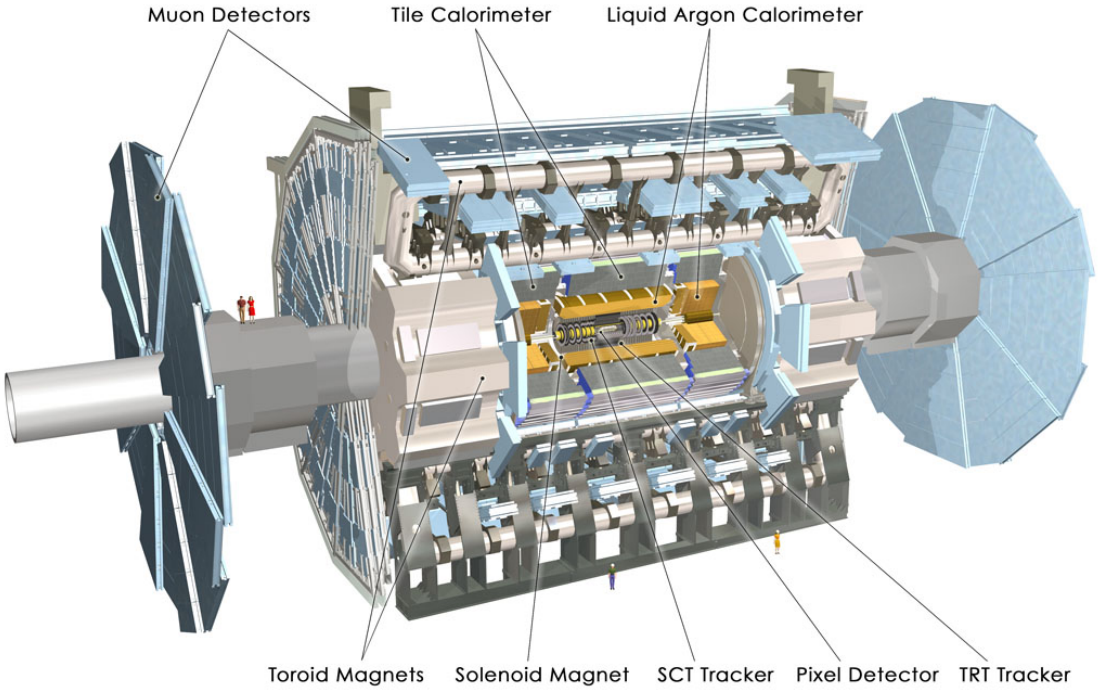

FIGURE 2.3: ATLAS detector scheme

component	**Resolution**	η	**trigger** (η)
Tracking	$\sigma_{p_T}/p_T = 0.05\% \times p_T \oplus 1\%$	$\lvert\eta\rvert < 2.5$	-
EM calorimeter	$\sigma_E/E = 10\%\sqrt{E} \oplus 0.7\%$	$\lvert\eta\rvert < 3.2$	$\lvert\eta\rvert < 2.5$
Hadronic calorimetry			
barrel and end-cap	$\sigma_E/E = 50\%\sqrt{E} \oplus 3\%$	$\lvert\eta\rvert < 3.2$	$\lvert\eta\rvert < 3.2$
forward	$\sigma_E/E = 100\%\sqrt{E} \oplus 10\%$	$\lvert\eta\rvert < 4.9$	$\lvert\eta\rvert < 4.9$
Muon spectrometer	$\sigma_{p_T}/p_T = 10\%@p_T = 1TeV$	$\lvert\eta\rvert < 2.7$	$\lvert\eta\rvert < 2.4$

TABLE 2.1: General Detector Performance

- Reconstruction of tracks for $|\eta| < 2.5$.
- The angles θ are measured with a precision of, at least, 2 mrad.
- The primary vertex is found along the z axis with an accuracy better than 1mm.
- The identification of electrons with $p_T \geq 7$ GeV is greater than 90%.
- Identification of photons combined with the electromagnetic calorimeter
- Identification of jets from b-quark.

The Inner Detector has three parts, the Pixel Detector, the Semiconductor Tracker (SCT) and the Transition Radiation Tracker (TRT). All contained on a 2T magnetic field that bends charged particles trajectory to allow measurement of the particles momenta (Figure 2.4).

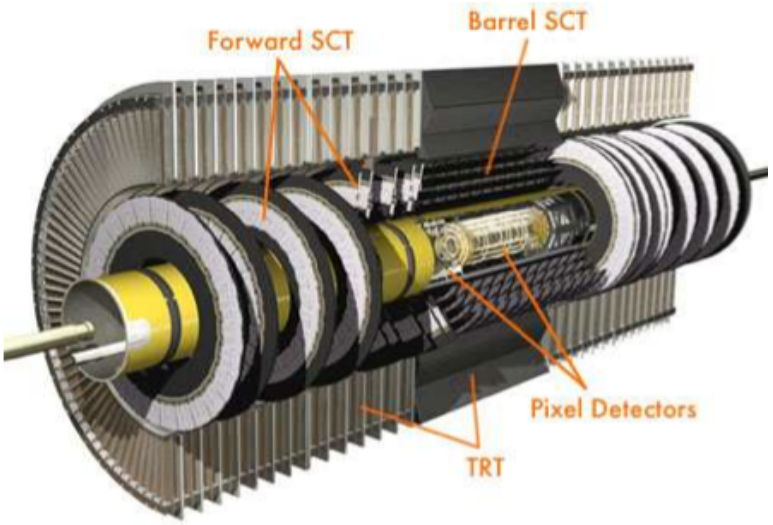

FIGURE 2.4: Inner Detector

2.2.2 Calorimeters

There are two calorimeters in the ATLAS detector: the electromagnetic and the hadronic, covering the regions $|\eta| < 3.2$ and $|\eta| < 4.9$, respectively (Figure 2.5). The electromagnetic calorimeter allows a precise measure of the energy and position of the electrons and photons that interact through electromagnetic force while the hadronic absorbs the energy of particles that interact through the strong force, after crossing the electromagnetic calorimeter. The hadronic calorimeter is meant to detect the particle shower resulting from the hadronization of the quarks, also known as jet, allowing to measure the energy of the original particle after calibration.

The EM calorimeter [3, 4] is a sampling calorimeter made of layers of lead (used as the passive material). Between the layers, liquid argon (LAr) is used as the active material. The accordion geometry provides complete ϕ symmetry without azimuthal cracks. It is divided into three regions: the barrel ($|\eta| < 1.475$) and two end-caps ($1.375 < |\eta| < 3.2$). It has the following properties:

- An angular coverage as large as possible to collect a maximum of rare events and to measure the missing energy.
- An excellent resolution on the energy in the order of 1%.
- A precise measurement of the direction of electromagnetic showers.
- An excellent separation of γs.

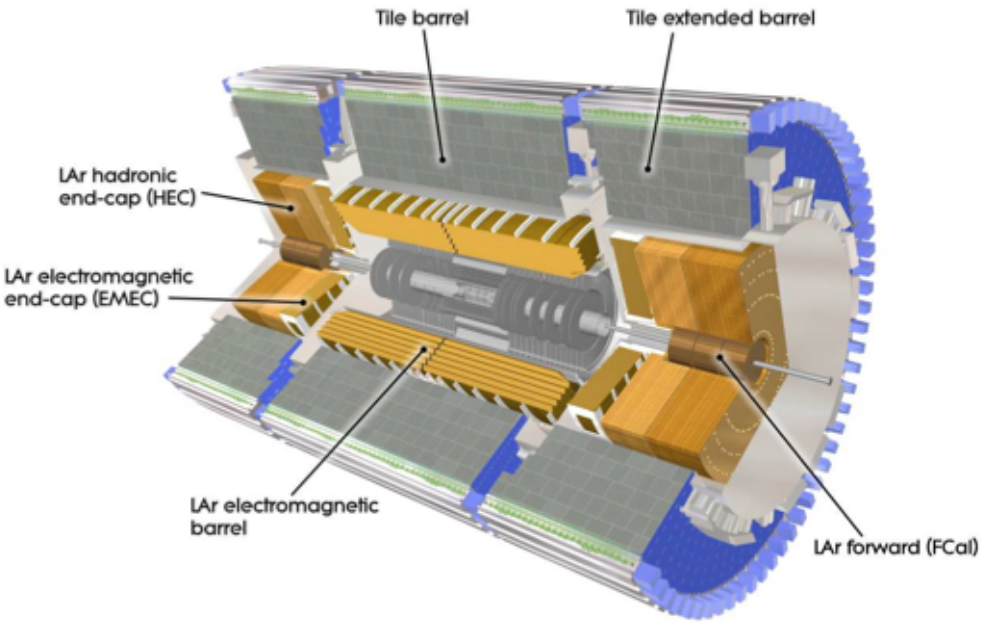

FIGURE 2.5: Calorimeter sub-detectors

The hadronic calorimeter is composed by three sub-detectors: the tile calorimeter (TileCal), the LAr hadronic end-cap calorimeter (HEC) and the LAr forward calorimeter (FCal). The TileCal [5, 6] is a sampling calorimeter using steel as the absorber and scintillator as the active medium. It is located in the region $|\eta| < 1.7$, behind the LAr EM calorimeter, and it is subdivided into a barrel central region ($|\eta| < 1.0$) and two extended barrels ($0.8 < |\eta| < 1.7$). The light produced in the scintillating tiles is collected at the edges of each tile using two wavelength shifting fibers that conduct the light to photomultipliers. The HEC covers the region $1.5 < |\eta| < 3.2$ overlapping the forward calorimeter. Each HEC consists of two wheels with a radius of 2.03m, each with 32 modules, and is divided in two longitudinal segments. Finally, the FCal is located at 4.5m from the interaction point covering the region $3.1 < |\eta| < 4.9$ with the main purpose of minimising the loss of energy and reduce background radiation levels in the muon spectrometer. FCal and HEC use cooper as the absorber and LAr as the active material. Its properties are:

- The identification of jets, the measurement of their energy and their direction.
- Good coverage in η to measure precisely the missing transverse energy.
- A good granularity.
- A linear response in energies for $|\eta| < 3$.

2.2.3 Muon spectrometer

The muon spectrometer is the last layer of ATLAS detector, has a cylindrical shape and measures 22m of diameter and 46m long. It has a full coverage in the region $|\eta| < 2.7$, with the exception of a region around $\eta = 0$, where a 300mm gap is present, allowing for the passage of the services for the ID detector, solenoid and calorimeters. This gap leads to a significant degradation of the muon reconstruction efficiency in that region. The Superconductors generate a magnetic field perpendicular to the trajectory of muons. The spectrometer measures the deviation to determine the momentum of muons.

To efficiently identify and measure muons, the Muon Spectrometer is composed by four different tracking detector technologies: Monitored Drift Tubes (MDT) and Cathode Strip Chambers (CSC) precision detectors in the barrel and end-cap regions; Resistive Plate Chambers (RPC) and Thin Gap Chambers (TGC) that provide fast trigger signals in the barrel and end-cap regions (Figure 2.6).

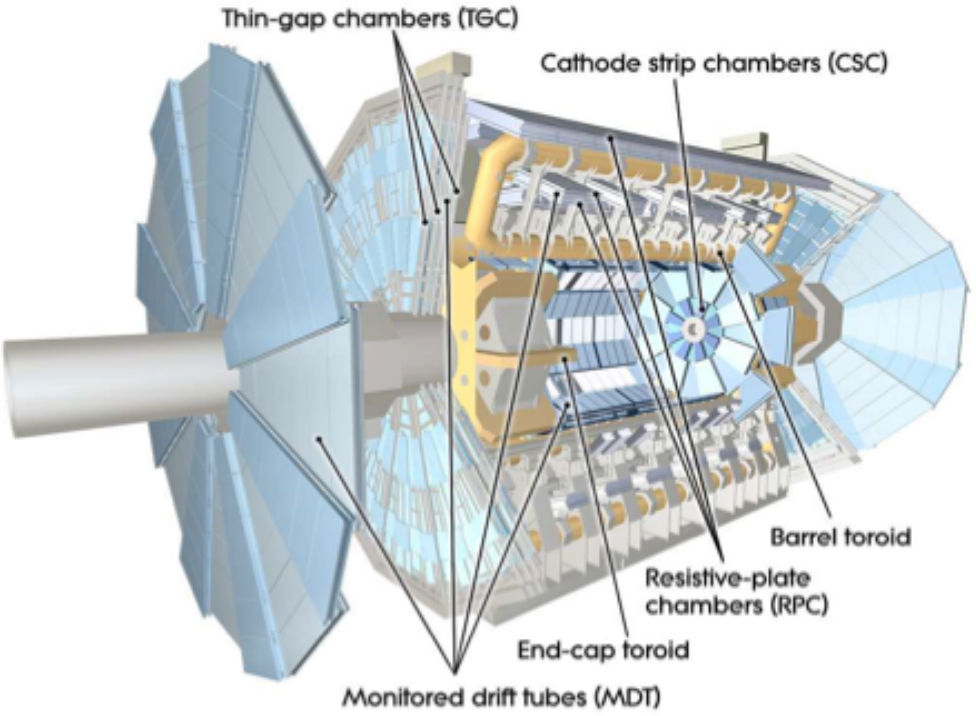

FIGURE 2.6: Muon spectrometer

The goals of this sub-detector are:

- A good resolution on the measurement of the transverse momentum for 5GeV<E <1 TeV.

- A good reconstruction of the muons tracks.
- Good angular coverage ($|\eta| < 3$).
- Ability to function in standalone mode (without the tracker).

2.2.4 Magnet system

Apart from the three main sub-detectors, ATLAS, has a system of four large superconducting magnets with the purpose of bending the charged particles produced in the events, allowing to measure their momentum and charge sign. The ATLAS magnet system consists of a solenoid, aligned with the beam axis, providing a 2T axially symmetric magnetic field for the inner detector; a barrel and two end-cap toroids, which produce a toroidal magnetic field of 0.5T and 1T, respectively, for the muon detectors. Figure 2.6 shows the geometry of the magnet system.

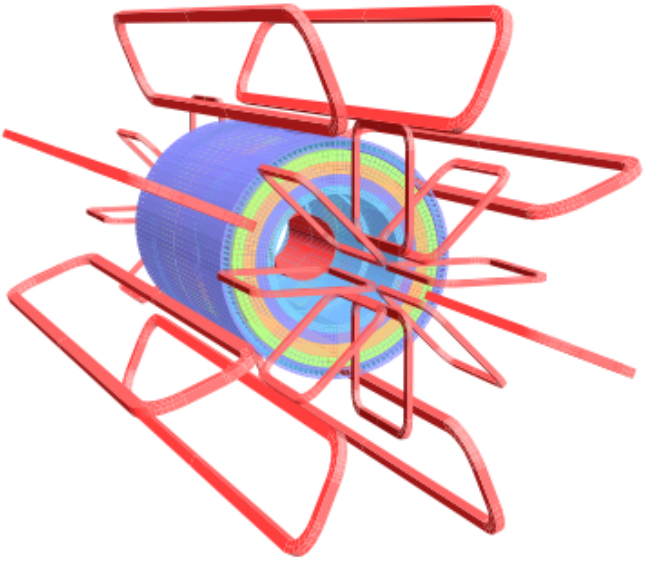

FIGURE 2.7: Magnet system

2.2.5 Trigger and data acquisition systems

The selection of events in ATLAS is done on three levels of trigger, based on the signatures of high-p_T particles and missing transverse energy. Each level allows to refine the selection in order to pass from a frequency of events of 10^9Hz to a frequency of storage of 100Hz. The trigger will therefore provide a factor of rejection of about 10^7.

The level 1 trigger will select high p_T muons, electrons, photons, jets and τ leptons decaying in hadrons. The decision time of 2μs includes the transmission of signals between the detector and the trigger electronics. After the 1^{st} has accepted an event, the data is read out, formatted and stored in buffers, being available to the next levels. The level 2 trigger uses about 2% of total event data at full granularity and precision, and it will reduce the trigger rate to 3.5kHz. At this stage, the processing time for an average event is 10ms. At final stage the rate will be reduced to 100Hz.

2.2.6 GRID

The LHC computing Grid is a distribution network designed to handle the massive amounts of data produced by the Large Hadron Collider (LHC). It incorporates both private fiber optic cable links and existing high-speed portions of the public Internet. The data stream from the detectors provides approximately 300 GB/s, which is filtered for 'interesting events', resulting in a 'raw data' stream of about 300 MB/s. This makes more than 1PB of data per year. The storage and offline reconstruction of this amount of data require the use of a large storage and computing resources. The Grid sites are organized in Tiers: the Tier-0 is located at CERN (where the data is produced) and it is connected via high-speed networks to eleven Tier-1 sites (located in different countries), which will store the output of event reconstruction. The Tier-1 centres will make data available to more than 150 Tier-2 centres, each consisting of one or several collaborating computing facilities, which can store sufficient data and provide adequate computing power for specific analysis tasks. Individual scientists will access these facilities through Tier-3 computing resources, which consist of local clusters (or even individual computers).

Chapter 3

TileCal and its calibration

The TileCal is a sub-detector of ATLAS as explained in the previous chapter. It is made of three aligned barrels. Both barrels on the exterior are the extended barrels. They measure 2.91m in length and cover the following range of pseudo-rapidity: $0.8 < |\eta| < 1.7$. The central barrel is called the Long Barrel and is 5.64m long, covering the pseudo-rapidity range $|\eta| < 1$. All three sections are subdivided into 64 independent modules. Each module covers a portion of $2\pi/64$ angle in ϕ that gives the granularity in ϕ. Radially, the modules are divided into three layers (Figure 3.1): A, BC and D. They correspond, respectively, at 1.4, 3.9 and 1.8 interaction length. The granularity $\Delta\eta \times \Delta\phi$ of the TileCal is 0.1×0.1 for the first two layers and 0.2×0.1 for the third layer.

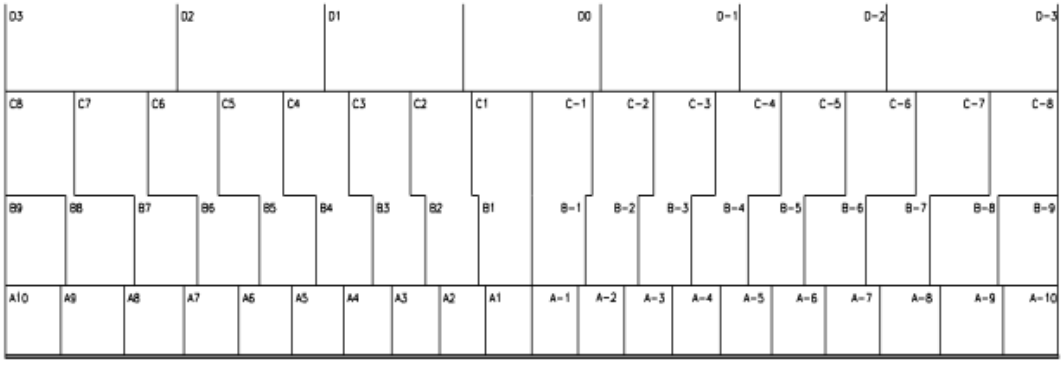

FIGURE 3.1: Different layers of a module of TileCal

The calorimeter measures only a fraction of the energy deposited by the incoming particles (it is a sampling calorimeter). The absorber plate is iron, while the active medium is constituted of scintillating tiles. The particles deposite a fraction of their energy in the scintillating tiles, which is converted into light. The light is transported by wavelength shifting fibers, placed on each side of scintillating tiles. The absorption spectrum of

the fiber is adapted to the wavelength of light produced in the scintillating tiles. The emission spectrum has been tailored to the absorption efficiency of the Photomultipliers (PMTs). PMTs are placed on the other end of the fiber converting the light into electrical signals. The charge collected by each PMT is then digitized and passed to the ATLAS readout system, allowing to double reading each cell. The scintillating tiles are placed in a plane perpendicular to the beam, and this geometry allows for the connection of optical fibers on the side outside of the module. Figure 3.2 represents a section of a TileCal module.

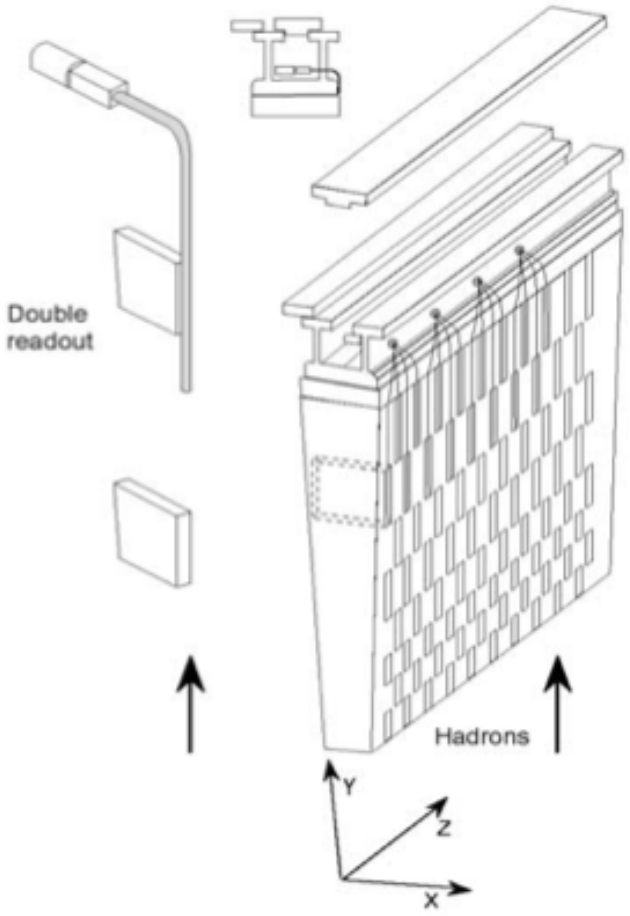

FIGURE 3.2: Section of a TileCal Module

3.1 Calibration of TileCal

In order to reach good physics analysis, the difference between the energy of the particle and the energy we are reconstructing should be as small as possible. This is the role of the calibration which can be made in two ways[11]:

- **Hardware**: a quantitative understanding of the TileCal response requires monitoring and control of a large number of parameters such as electronic noise, PMT gain, among others, which in turn depend on a large number of variables (time, temperature,...). All such parameters must be known precisely in order to correctly interpret the data collected. Consequently, all these parameters have to be measured precisely and integrated into the calibration system.
- **Software**: once the hardware calibration has been performed, one still has to correctly estimate the shower energy. The calorimeter finite granularity will lead to a non-exact estimation of the shower energy, even with a perfect hardware calibration. This is sorted out using specific software corrections.

There are three main components in the TileCal calibration scheme (Figure 3.3) - the Cesium system, the LASER system and the charge injection system (CIS). With those 3 systems we achieve a complete calibration of the hardware chain, from the active modules to the read-out electronics.

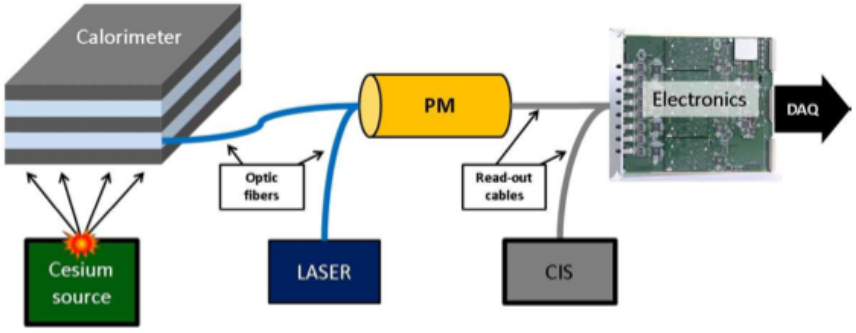

FIGURE 3.3: Hardware calibration chain

3.1.1 Cesium System

A ^{137}Cs source is moved inside the calorimeter modules during ATLAS shutdown periods via a complex network of pipes filled with water. The light thus produced is collected and measured for each cell, leading to the comparison of each TileCal cell response. In Figure 3.4 is shown the response of 5 cells during the passage of the Cesium source. Each secondary peak represents the passage of the source through a tile. In this case, for the second cell, there is an absence of a peak. This is due to poor coupling between the fiber and the scintillating tile. With the detection of such a flaw one can make a repair. However since the signal passes through the full data aquisition chain if the Cesium sees a drop in one cell efficiency, it could be due to different sorts of problems,

for example a gain variation in the PMTs. We thus need other systems in order to solve this uncertainty.

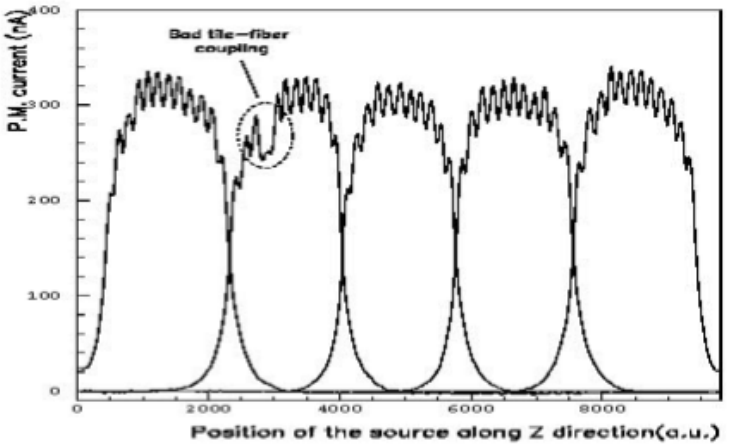

FIGURE 3.4: PMT current as a function of source position for 5 adjacent cells

The Cs system provides a calibration of the full readout chain.

3.1.2 LASER system

The LASER system is the next in the chain and was designed to calibrate and monitor the PMTs response with an accuracy better that 0.5%. The LASER pulse produces a similar PMT response as a signal generated by a particle in the TileCal. The major difference is that the initial energy of the light pulse is known precisely (better than 1%). This enables accurate monitoring of PMT gains and linearity.

The LASER system is divided into two main parts: the LASER box and the light distribution system.

3.1.2.1 LASER box

The LASER box (in Figure 3.5) contains not only the LASER head, but also two PMTs used for triggering and monitoring purposes, four Si PIN photodiodes (inter-calibrated by a ^{241}Am source) used for the absolute measurement of the light intensity emitted by the LASER, and the optical circuitry necessary for changing the LASER beam intensity. The humidity and temperature in the box are constantly monitored and controlled.

The LASER light is transmitted to the photodiodes via four optical fibers connected to the box. One out of the four fibers (the one linked to diode number 1) is receiving

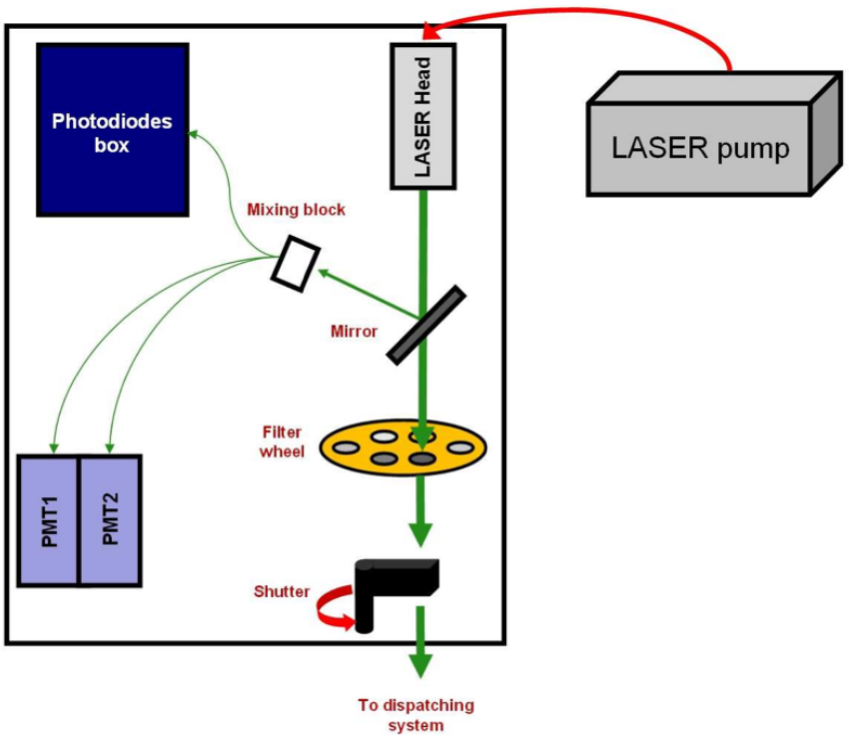

FIGURE 3.5: The Laser box

light collected directly in the LASER box, whereas the others are getting information at another level of the system. Diode 1 and the two PMTs (which are similar to the PMTs installed in the TileCal) receive light via a semi-reflecting mirror.

The light that is not reflected by the mirror passes through a filter wheel with 8 holes. One of them is empty (position 5) while the others contain filters providing beam attenuation with a factor 3 to 1000. The design values of the filter attenuations are in Table 3.1. These filters were chosen to provide full coverage of the entire TileCal dynamic range, from a few hundred of MeV to around 1TeV.

Position	1	2	3	4	5	6	7	8
Attenuation	1050±350	103±23	32±6	10±1	1	3.1±0.2	103±23	330±100

TABLE 3.1: Filter wheel attenuation factors

In the Laser box there is also a shutter, which was installed for safety reasons and is closed when the LASER is not in use. It can be used to make tests without sending light to the TileCal.

3.1.2.2 Light Distribution System

If a LASER pulse is emitted when the shutter is opened, the light exits the LASER box and enters into a 1m long liquid light guide. It links the LASER box output to the first component of the light distribution system - the beam expander (Figure 3.6). It is a system composed of two lenses that expand the beam diameter. It also has a diffuser in order to prevent effects due to LASER light coherence. The Coimbra box in turn sends the primary beam toward a bunch of 384 clear fibers (128 for each end-cap barrel, and 128 for the long barrel).

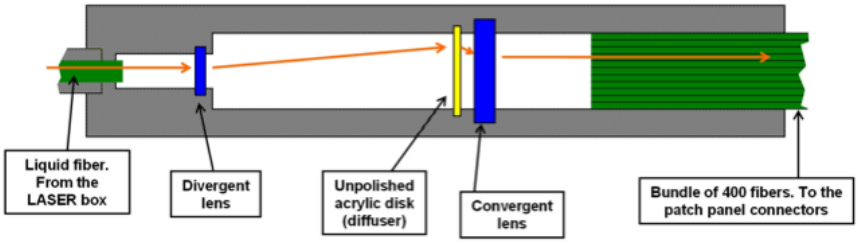

FIGURE 3.6: Beam expander

Each fiber is glued to an adjustable connector that is held in a big patch panel located immediately behind the LASER box. The role of the connectors is to equalize the light sent by all the fibers to the TileCal. The fact that all PMTs receive roughly the same light amount simplifies the calibration work.

At the other side of the connectors, long clear fibers take the light individually to TileCal drawers where they are split a last time in order to reach all the PMTs. Each extended barrel is fed by two fibers (17 PMTs per fiber) and each barrel module (two partitions) is fed by two fibers (45 PMTs per fiber). This is summarized in Figure 3.7.

Again, not all of the fibers coming out of the Coimbra box go to the TileCal. Around 20 fibers are either kept as spares, or used to feed the three remaining diodes in the LASER box.

This system is fast enough to be used in the acquisition phase. During each acquisition run the LASER will send pulses in the gaps of beam particle crossing. This is used to check, for example, the status of the PMTs during all the data acquisition run (Figure 3.8).

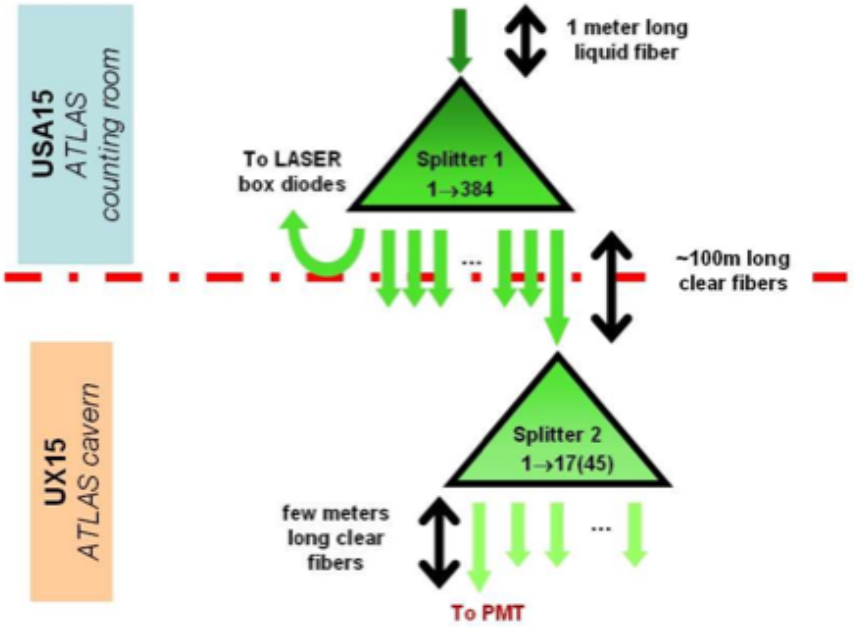

FIGURE 3.7: The light distribution system

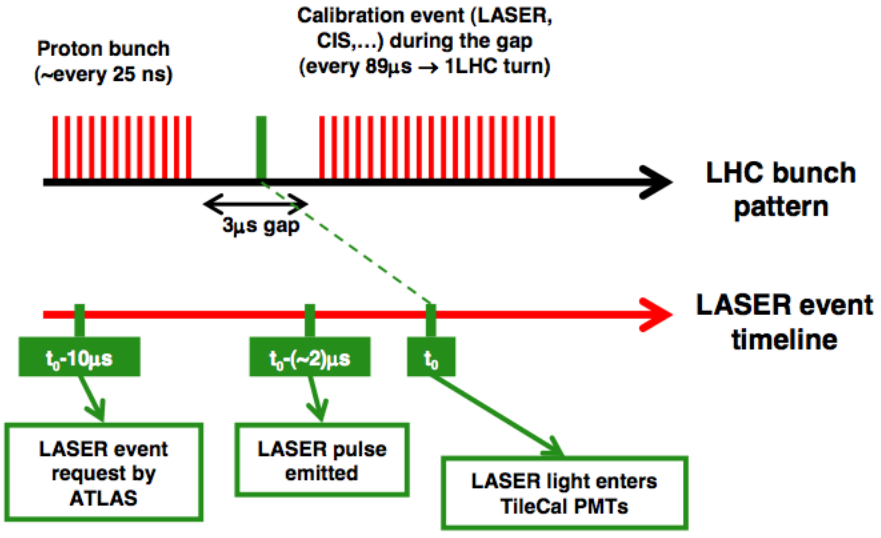

FIGURE 3.8: Calibration event during a gap

3.1.3 CIS

Change impulses of known intensity are pulsed into the readout electronic chain. These mimic the response of the PMTs in the electronics located ahead of the PMTs. It leads to a precise estimation of the electronic noise and linearity. Its objective is an accuracy of around 1%. In ATLAS there will be periodic CIS runs over the full dynamic range during maintenance periods. Also, in data acquisition phases, a fixed amplitude signal is injected when there are no crossings of particles, for calibration purposes. CIS calibrates the end side of the readout chain.

Chapter 4

Linearity studies using one LASER intensity and different wheel positions

The files being analyzed are ntuples coming from LASER runs with all sorts of information, such as the signal of TileCal PMT, the ADC of the LASER box four diodes and the two PMTs and respective pedestals, intensity of the LASER, temperature, etc. The runs used are: 129566, 129570, 129574, 130425, 130430, 130435 corresponding to the LASER intensities: 15k, 20k, 25k, 15k, 20k, 25k respectively.

The linearity plots will be made plotting the signal of a PMT of the TileCal against the reference signal (Diode 1 or PMT 1). Since the signal from the references comes from the LASER light reflected by the mirror that is never attenuated by the filter wheel (as explained in chapter 3), that attenuation factor needs to be taken into account to scale the reference signal and make the plot.

The first thing to do is to convert the histograms from each TileCal PMT and the reference signal used (Diode 1 or PMT 1 of the LASER box) to a mean value. This is done fitting a gaussian function to the histogram and taking the p1 parameter (mean) as shown in Figure 4.1. Selecting only the signals in the interval 0.1-700pC and 50-2050ADC for the TileCal PMTs and the PMTs or diodes of the LASER box respectively.

$$f(x) = p_0 e^{-\frac{1}{2}\left(\frac{x-p1}{p2}\right)^2} \tag{4.1}$$

The attenuation factors are computed as the ratio between the mean signal (from the fit described above) of a PMT using filter 5 (no attenuation) and the filter in question.

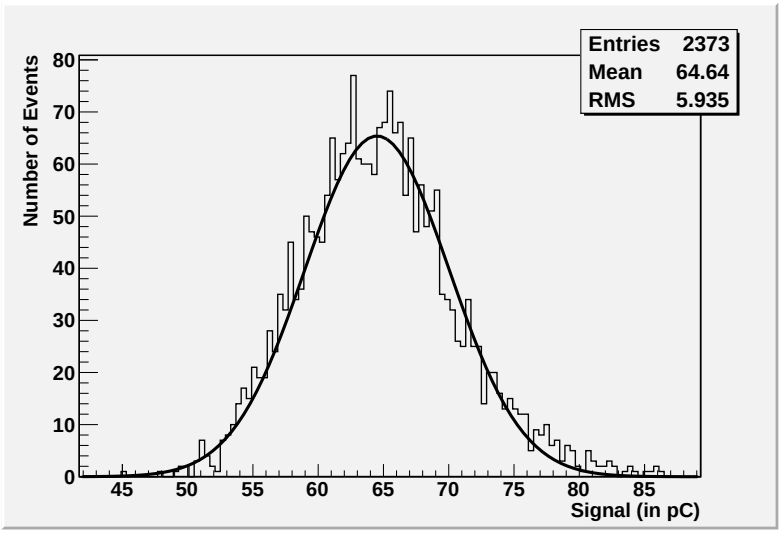

FIGURE 4.1: Gaussian fit for the signal of PMT_{000} for filter 5 and intensity 15k.

$$E_5 = F_i E_i \leftrightarrow F_i = \frac{E_5}{E_i}, i = \text{filters wheel positions} \tag{4.2}$$

Making an histogram with all the PMTs calculated factors for a given filter, one can fit a gaussian function again to get the mean value. The histograms for each filter are shown in Figure 4.2.

These values are within the ones provided by the manufacturer (Table 3.1).

Now, having the values for the PMTs signal and the reference signal (scaled with the attenuated factor) it is possible to make the linearity plot.

The plots with one and all the three runs were done (Figure 4.3) and it is evident that when we mix the three runs there are sources of systematic errors that increase the chi-square probability (χ^2/ndf and χ^2 probability plots in Figures 4.4 and 4.5 respectively). These problems will be addressed in chapter 5.

It is worth noting that even using only one run, the fit does not give good a χ^2 probability because the errors coming from each point are so small. In fact, looking at Figure 4.1 it is clear that the fit is done from a large sample of data, which makes the statistical errors very small. The errors used so far are rms/$\sqrt{n}$ and, as one can see, with such a large n the errors are very small.

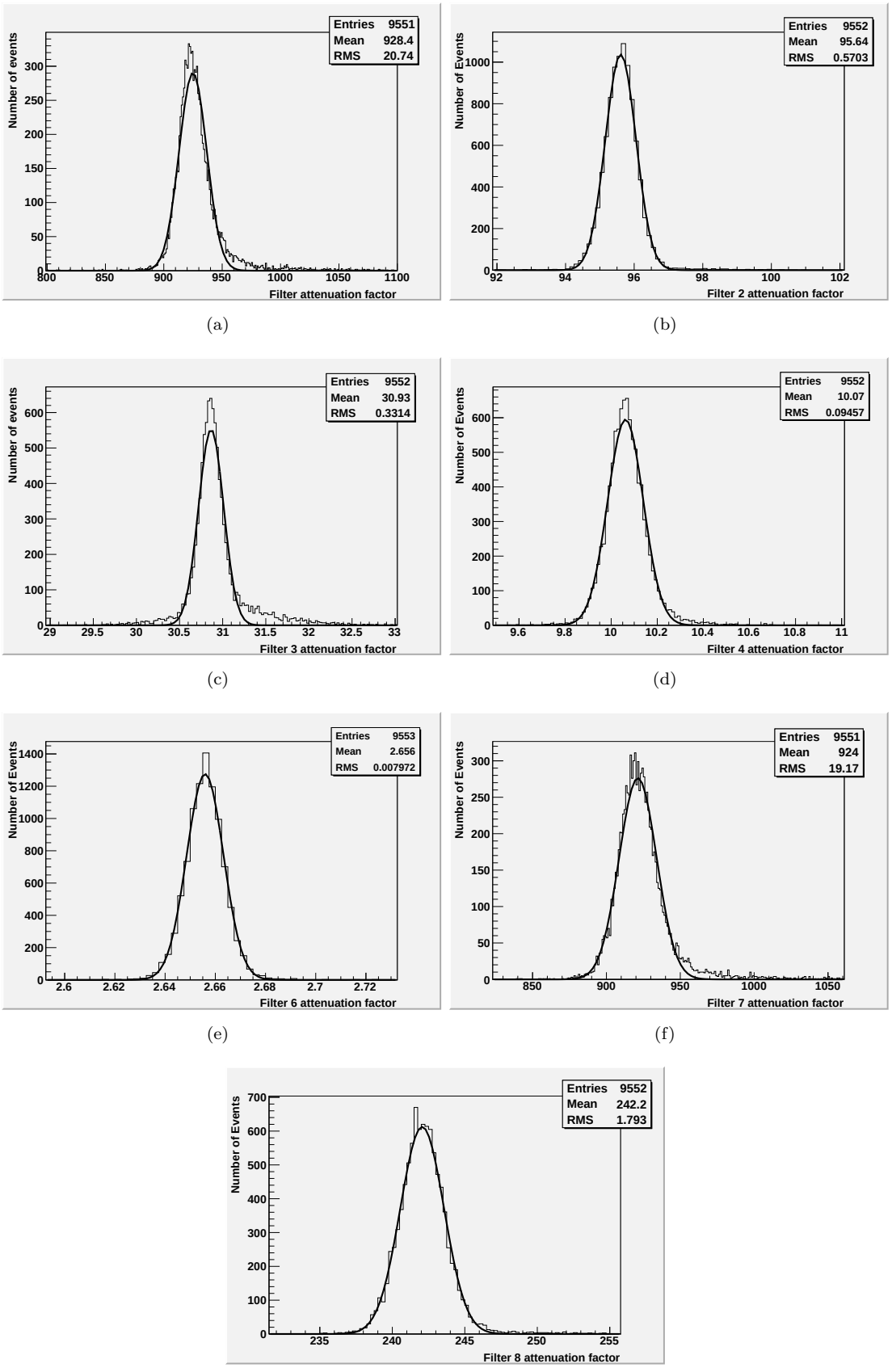

FIGURE 4.2: Histograms obtained from the attenuation factors from all the PMTs. a)Attenuation factor for filter 1, b) for filter 2, c) for filter 3, d) for filter 4, e) for filter 6, f) for filter 7, f) for filter 8.

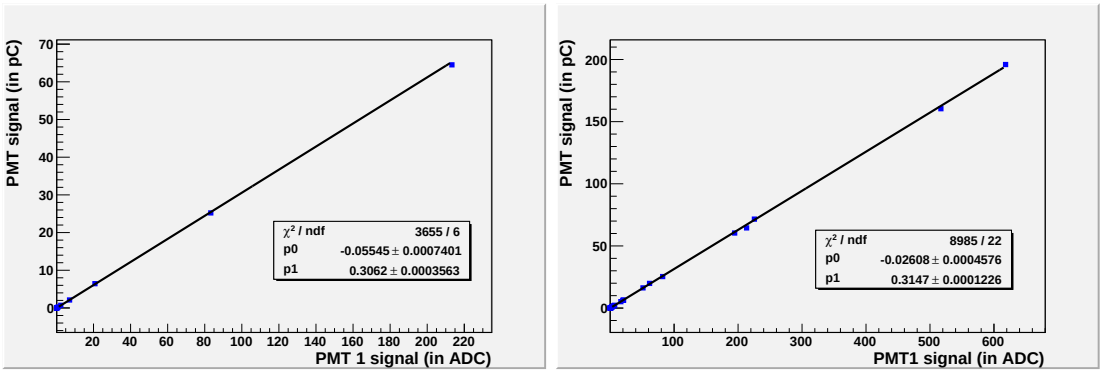

(a) (b)

FIGURE 4.3: Linearity plots for PMT_{000} with a) 8 points using 1 run b) 24 points, 3 runs.

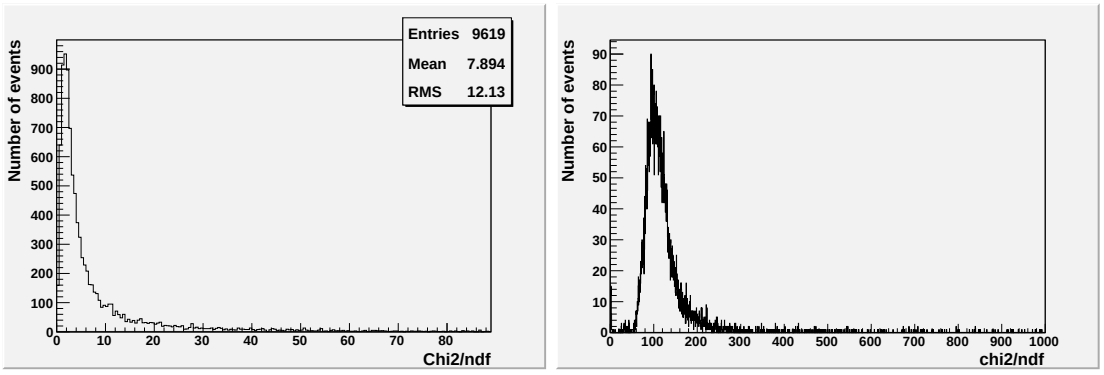

(a) (b)

FIGURE 4.4: χ^2/ndf a) using 1 run b) using 3 runs.

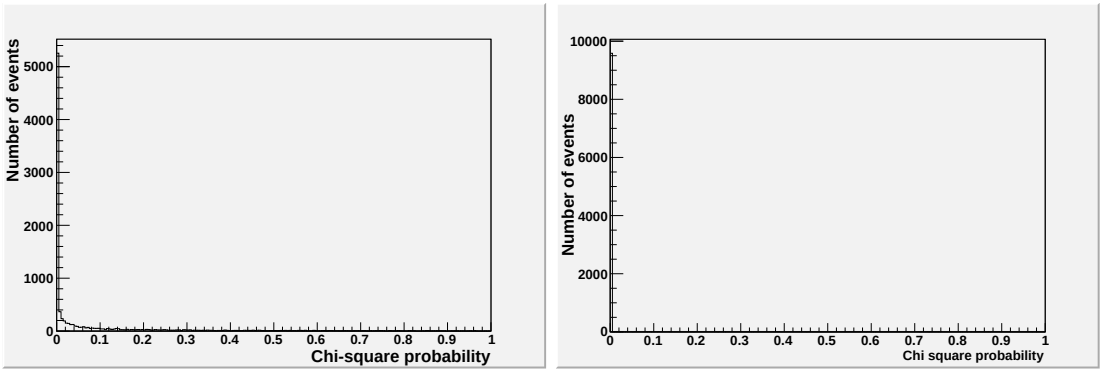

(a) (b)

FIGURE 4.5: χ^2 probability a) using 1 run b) using 3 runs.

4.1 PMT1 vs diode 1 as references

Another fact to note is that it was used so far the PMT1 as reference (instead of diode 1) because the diodes are affected by the light crosstalk effect [10] meaning so that the four of them are close enough to affect the signals of each other. While this is not a problem when making stability analysis, it becomes more serious for the linearity because the diodes signal will not be linear anymore.

Comparing the fits coming from plots with the PMT1 and the diode 1 as reference, one ends up with Figure 4.6.

From this results it cannot be observed the crosstalk effect as both references give very similar probabilities in the fit.

4.2 rms vs gaussian error

Another comparison that can be done is between using rms errors or the error from the gaussian fit in the mean parameter p1. As shown in Figure 4.7, there is some difference between the methods of errors used. However, it seems that there are no systematic effect.

4.3 Different intensities

Now, using PMT1 as reference (that does not suffer from the crosstalk), one could compare runs 129566, 129570, 129574 (15k, 20k and 25k) parameters plotted in Figures 4.8, 4.9 and 4.10. Although the probability plots do not seem to follow any pattern, since the fits continue to appear very bad, due to the very small statistical errors, there is an improvement in the fit, looking at the residuals. Low intensities, such as 15k (Figures 4.8 and 4.11) filters 1 and 7 and, to some extension, filter 8 (corresponding to larger filter attenuations or, in another way, weaker signals) give the bigger deviations from the fit. This is due to the non-linearity of the electronics[10] that occurs for signals <100pC. Since the signals are selected in the interval from 0.1 to 700pC the results show that effect. In the next chapter those values will not be considered. It is worth to point out that all the residuals are around zero meaning that they are not biased. The offset parameter is also around zero as expected. Looking at the residual values, and disregarding filter 1, 7 and 8 at low intensity, they are between around 1% to 2%.

Also comparing both 15k runs 129566 (Figure 4.8) and 130425 (Figure 4.11), and 20k run (Figure 4.9) and 130425 (Figure 4.12) the results are similar as it was expected.

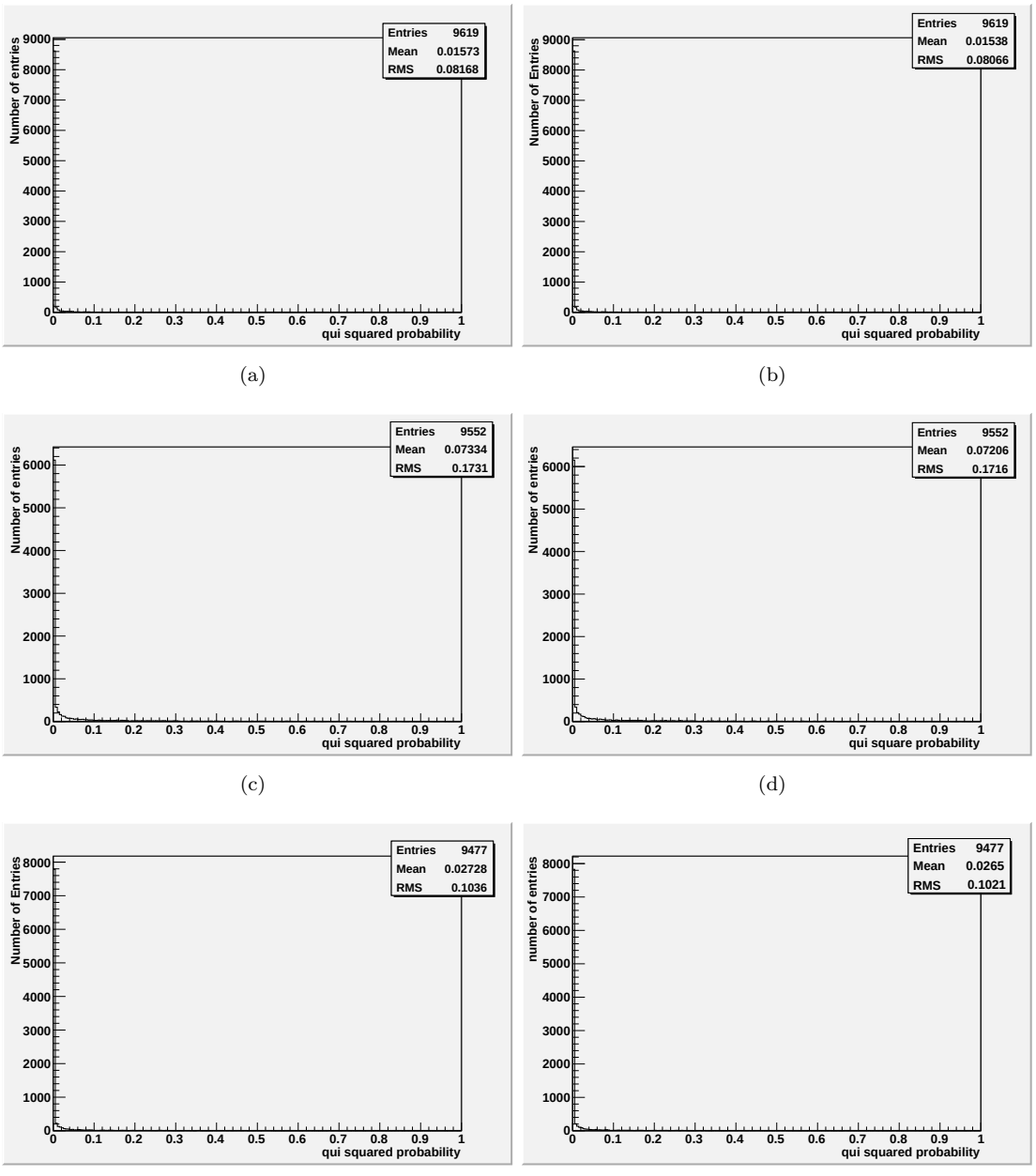

FIGURE 4.6: χ^2probability comparison using as references diode 1 and PMT1 a) 15k run using diode 1 as reference b) 15k run using PMT1 c) 20k run using diode 1 d) 20k run using PMT1 e) 25k run using diode 1 and f) 25k run using PMT1.

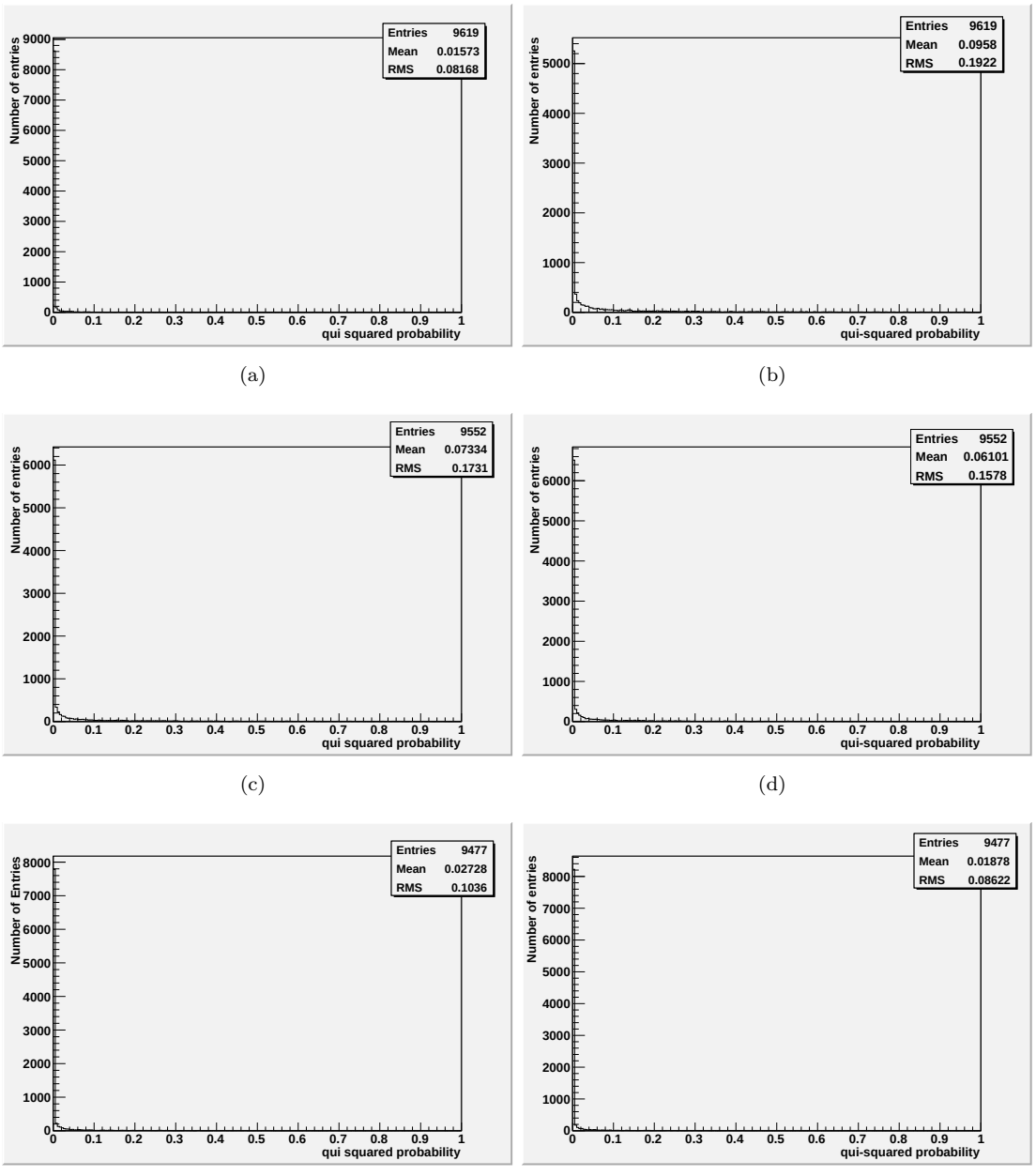

FIGURE 4.7: χ^2 probability comparison between rms error and gaussian a) 15k run using rms error b) 15k run using gaussian error c) 20k run using rms error d) 20k run using gaussian error e) 25k run using rms error and f) 25k run using gaussian error.

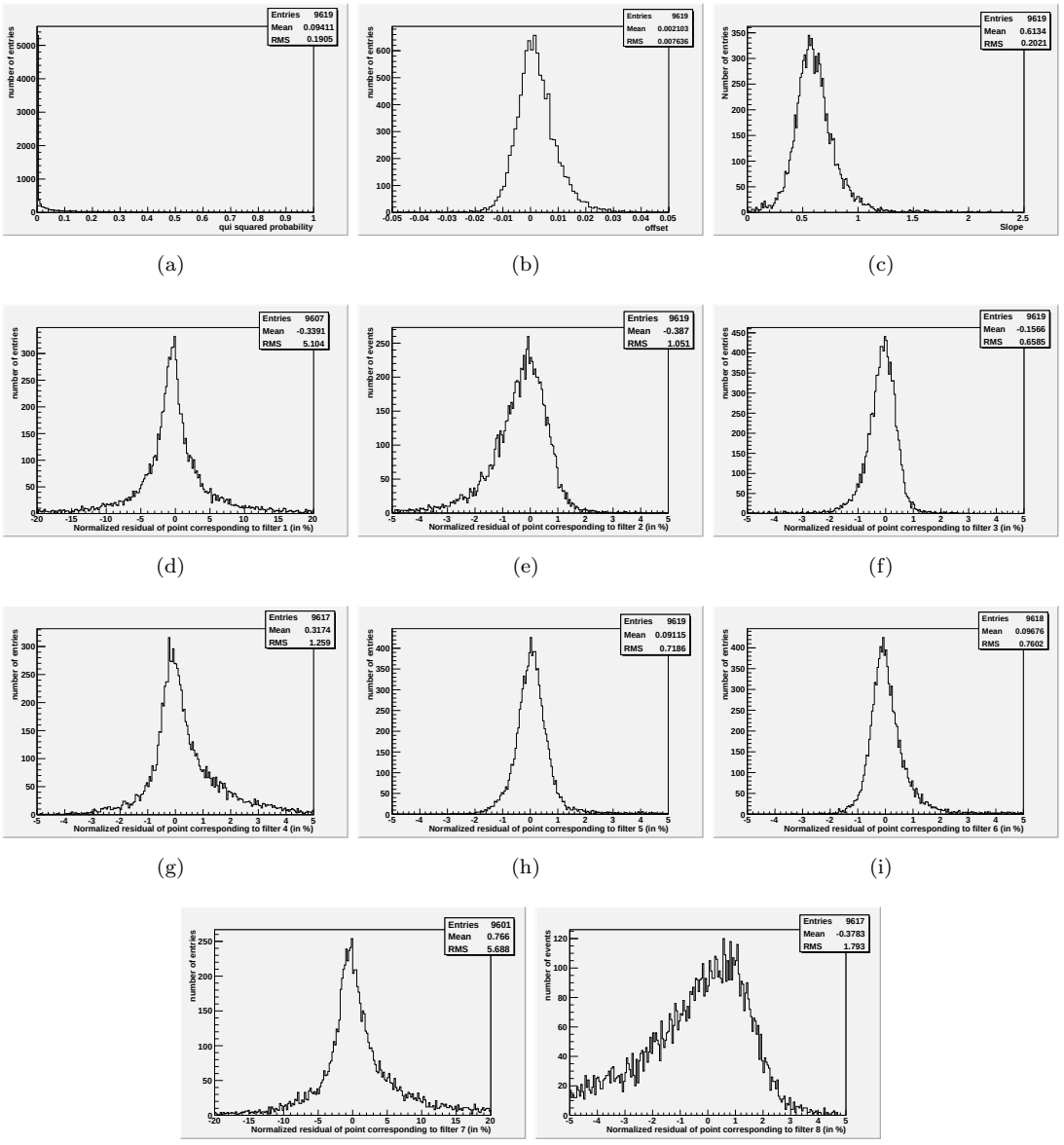

FIGURE 4.8: 15k run histograms (run 129566) a) the χ^2 probability, b) the offset parameter, c) the slope and d-k) the normalized residuals (in %) for the 8 filter wheel positions.

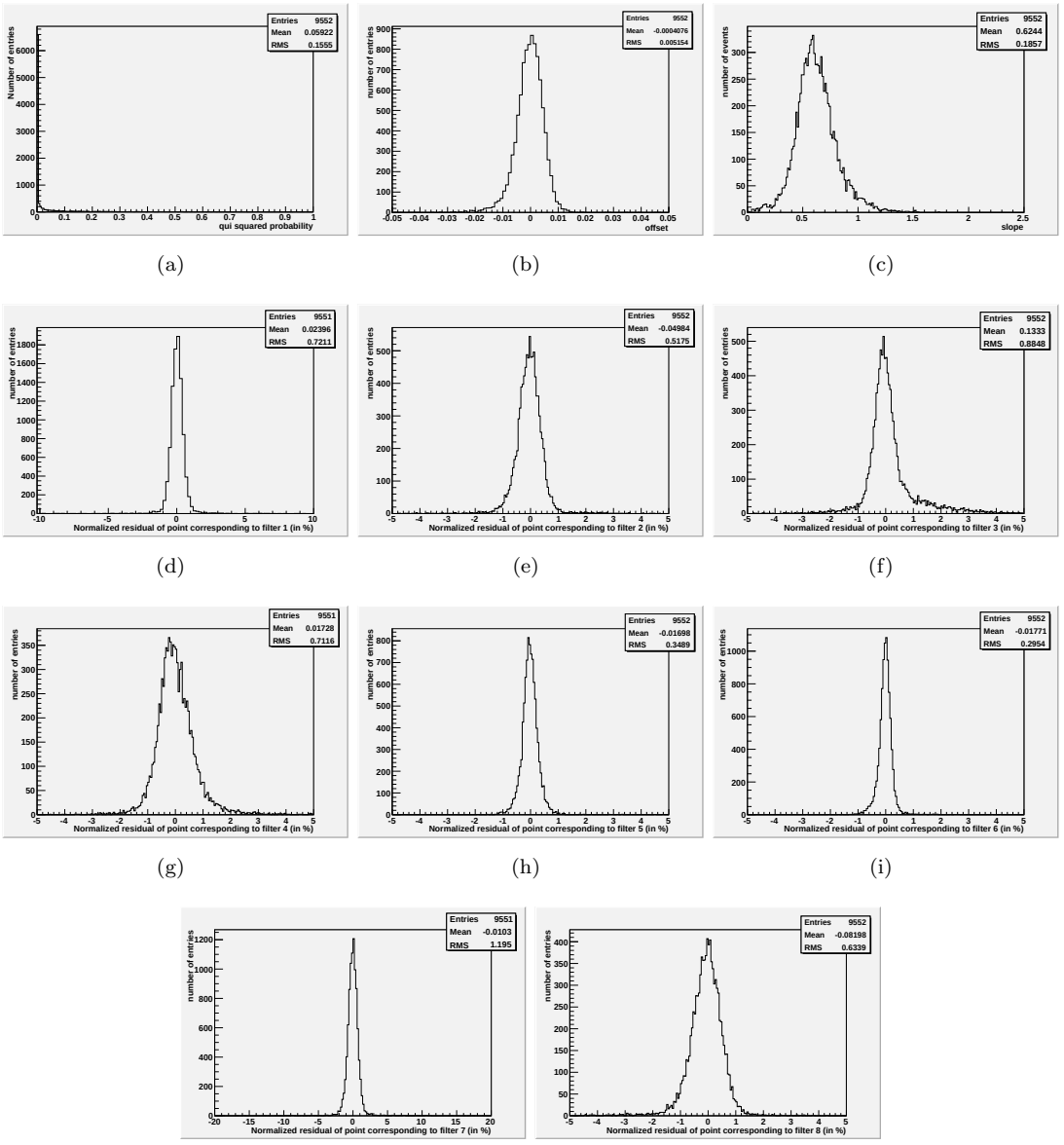

FIGURE 4.9: 20k run histograms (run 129570) a) the χ^2 probability, b) the offset parameter, c) the slope and d-k) the normalized residuals (in %) for the 8 filter wheel positions.

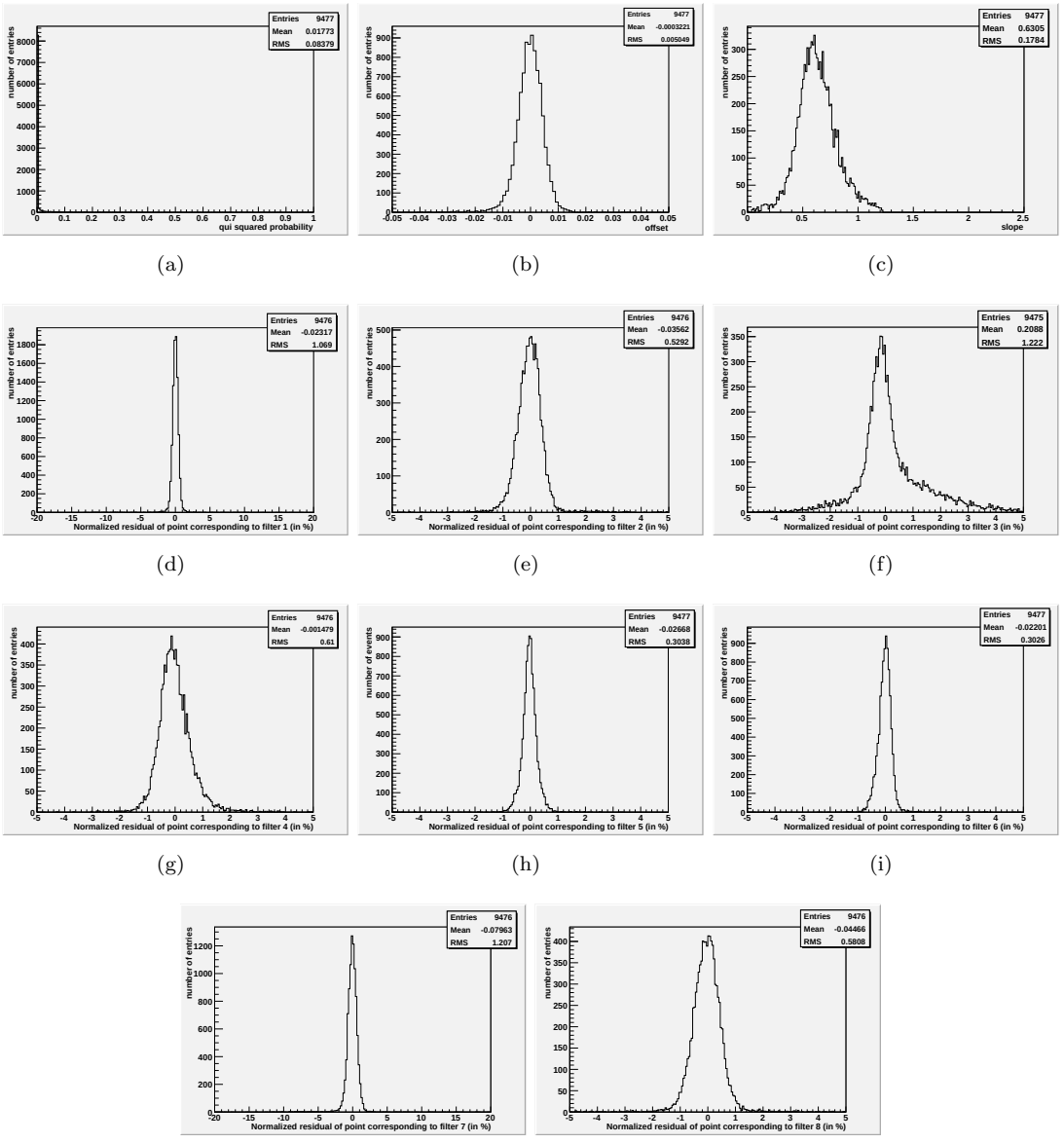

FIGURE 4.10: 15k run histograms (run 129574) a) the χ^2 probability, b) the offset parameter, c) the slope and d-k) the normalized residuals (in %) for the 8 filter wheel positions.

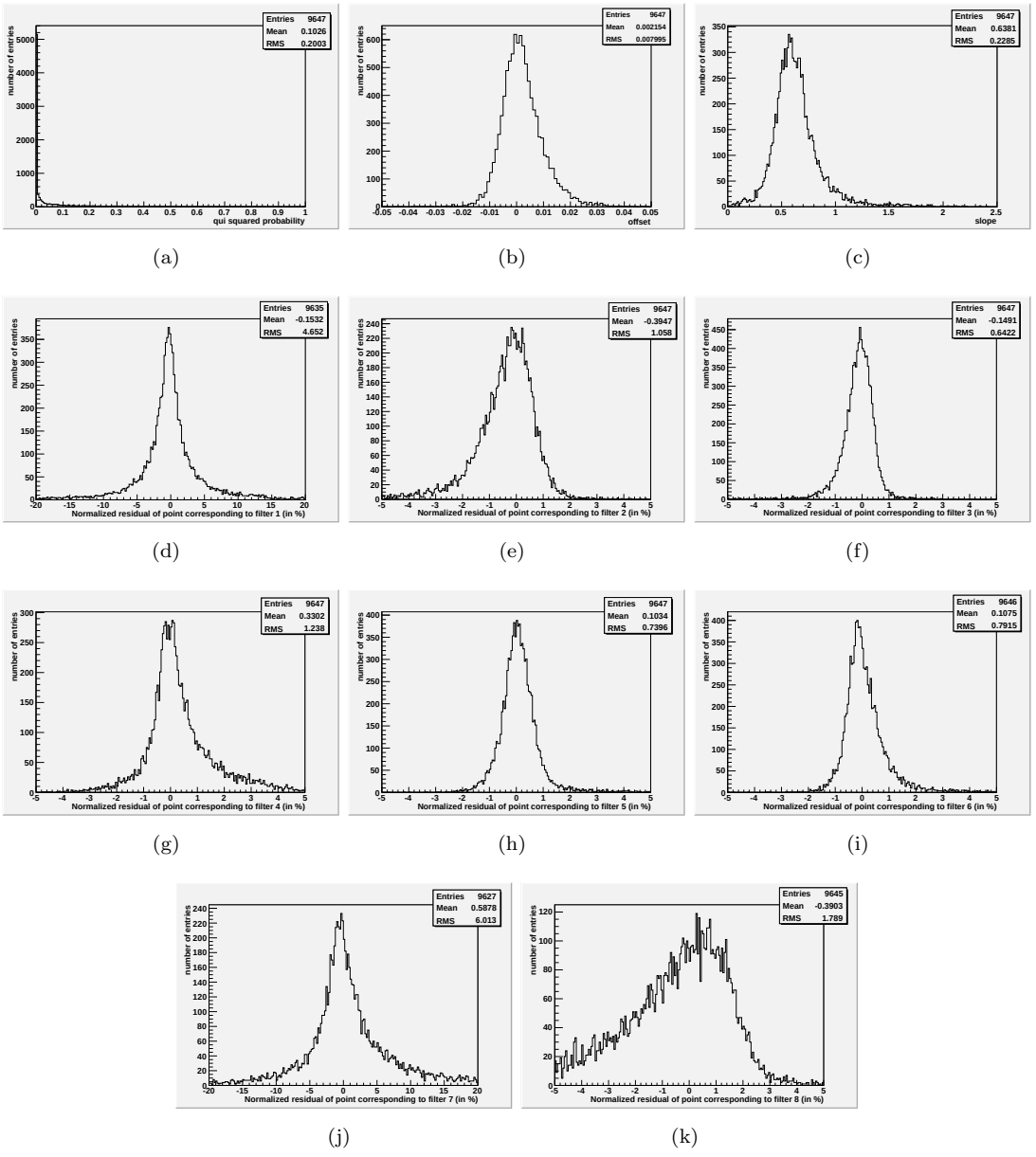

FIGURE 4.11: 15k run histograms (run 130425) a) the χ^2 probability, b) the offset parameter, c) the slope and d-k) the normalized residuals (in %) for the 8 filter wheel positions.

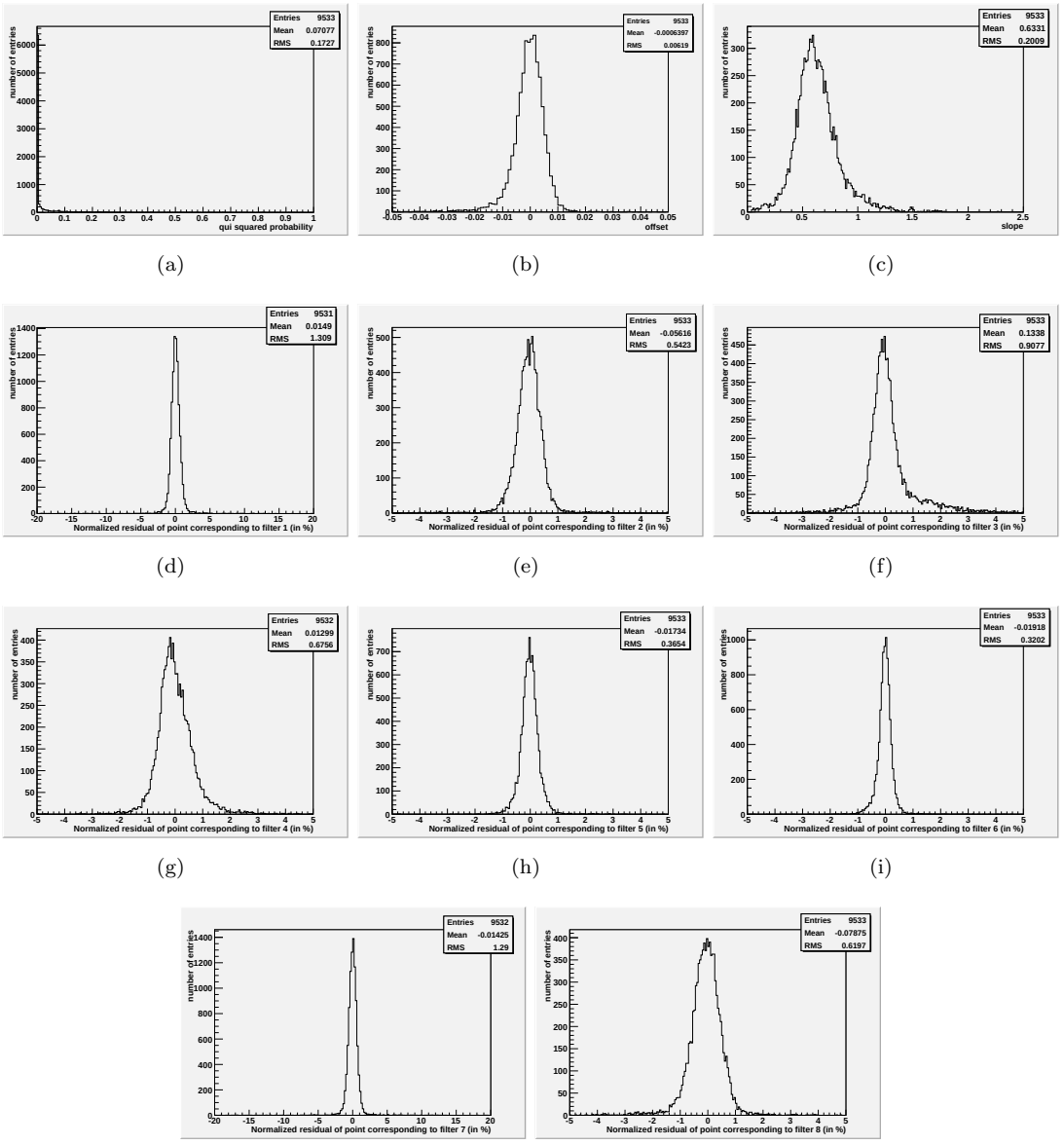

FIGURE 4.12: 20k run histograms (run 130430) a) the χ^2 probability, b) the offset parameter, c) the slope and d-k) the normalized residuals (in %) for the 8 filter wheel positions.

Chapter 5

Linearity studies using a single filter wheel position and different intensity runs

In chapter 4, results of linearity studies obtained with a moving filter wheel were discussed. The data show that the point by point fluctuations are larger than the statistical errors, producing bad χ^2 probability fits. The origin of the systematic errors can be studied using a simpler data taking configuration with a single filter position and different laser intensities. The results obtained are discussed in this chapter. Data with the filter wheel in position 5 (no light attenuation) and 8 intensities equal to 15k, 17k, 19k, 21k, 23k, 25k, 27k and 29k were used. Selecting only points with energy between 100 - 700 pC were eliminated the energy intervals in the region of the nonlinearity of the electronics (<100 pC) and the energies for which the PMTs start to saturate [10] . Additionally was removed all the PMTs flagged as having an identified bad behavior.

In Section 1, the results obtained using the LASER box PMT's (PMT1 and PMT2) were discussed. These results do not suffer from the light crosstalk effect. The linearity studies performed using the photodiode 4 are presented in section 2. Sections 3 and 4 are devoted to the results obtained using the PMTs of the TileCal to normalize.

The linearity results were obtained using the scatter plots PMT signal versus the signal of the reference counter. A typical example obtained using the PMT1 of the LASER box is shown in 5.1. The TileCal photomultiplier and reference signals were defined as the average of the corresponding distributions. The error is given by the ratio between the r.m.s. of the correspondent distributions and the square root of the number of histogram entries. Contrary to chapter 4 where the original ntuples were used and the parameters

calculated from the distributions, in this case they were already given by the calibration software.

As shown in 5.1 the data are fitted using the straight line function PMT = a.Sigref + b. Where Sigref is the normalization signal.

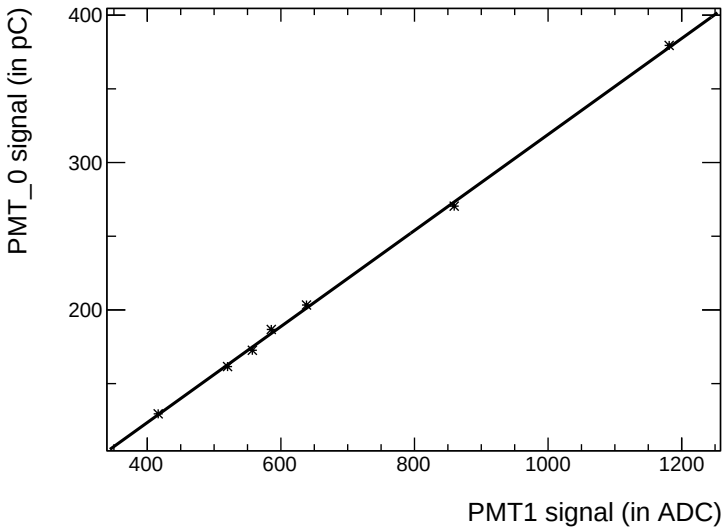

FIGURE 5.1: Example of a fit

5.1 PMTs vs PMT1

The results are shown in Figure 5.2. One can immediately see that the residuals of the points are biased: not centered at zero as they should. The same for the offset parameter. This indicates that there are some systematic effects that are shifting the points in some direction affecting the fits, resulting in bad chi-squares. This effect produces residuals that go up to 2% maximum.

The results can be explained if the PMT1 signal is not linear. Also there could be some kind of change in the Laser system itself in a way that 2 runs with the same intensity produce different output signals. Those hypothesis will be discussed in the next sections.

5.1.1 Linearity of the PMTs in the LASER box

The same set of runs was taken, this time with the shutter closed, so that no light passed to the PMTs of TileCal and to diodes 2 to 4, eliminating the crosstalk on diode 1. This

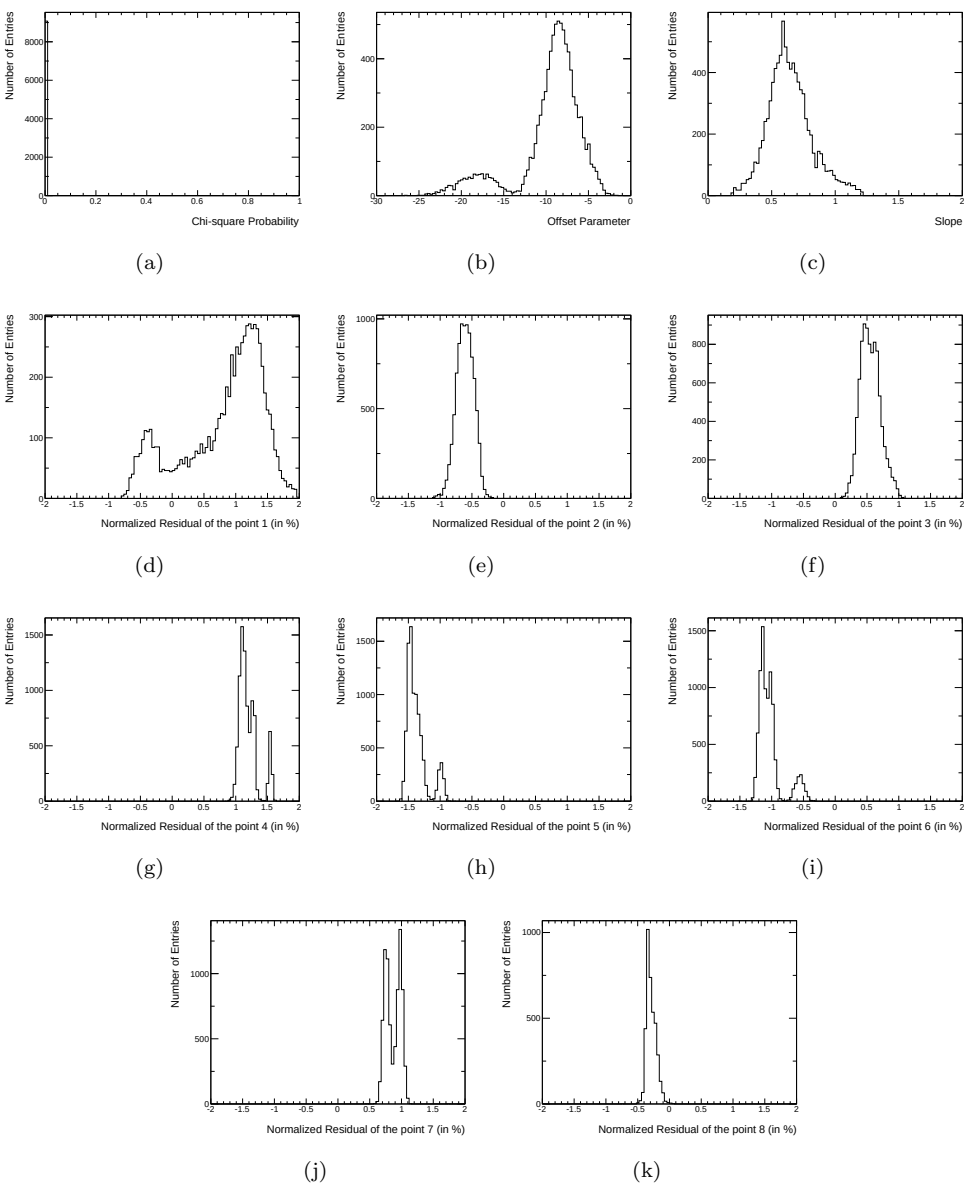

FIGURE 5.2: Histograms obtained in the study PMT vs PMT1. a) the chi-squared probability, b) the offset parameter, c) the slope, and d-k) The residuals (in %) of the points 1 to 8 that correspond to the intensities 14k to 23k.

one was assumed to be linear and thus used as reference. The plots PMT1/2 vs Diode 1 were produced and again the normalized residuals were calculated (Figure 5.3).

The χ^2/NDF is bad (11.4 for PMT1 and 22.2 for PMT2, and chi-square probabilities very low 10^{-11}, 10^{-22} respectively) but again, the statistical errors in each point are very small due the large number of entries. Looking at the residuals they are smaller than 0.5% so one can assume that the linearity of the PMTs of the Laser box is adequate.

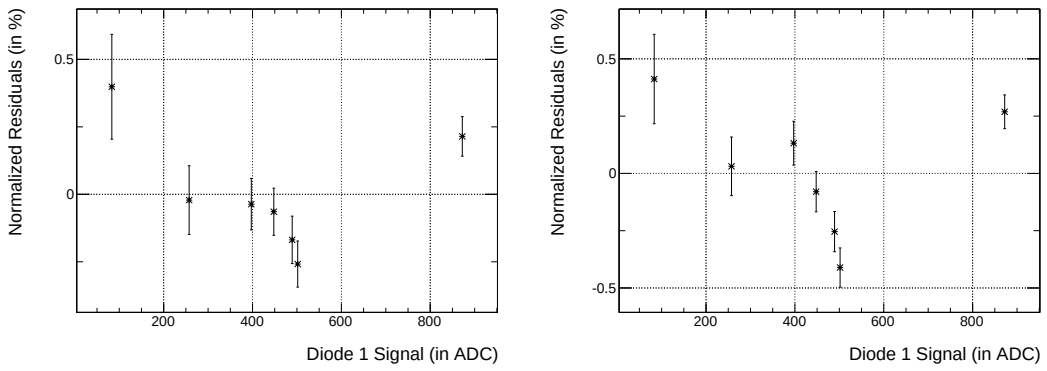

(a) PMT1 vs Diode 1 (b) PMT2 vs Diode 1

FIGURE 5.3: Linearity of the PMTs in the LASER box

5.1.2 Comparing runs with the same intensity

To try to understand the amplitude of the fluctuations, several runs were taken at 14k and 26k. The ratios PMT/PMT1 were computed.

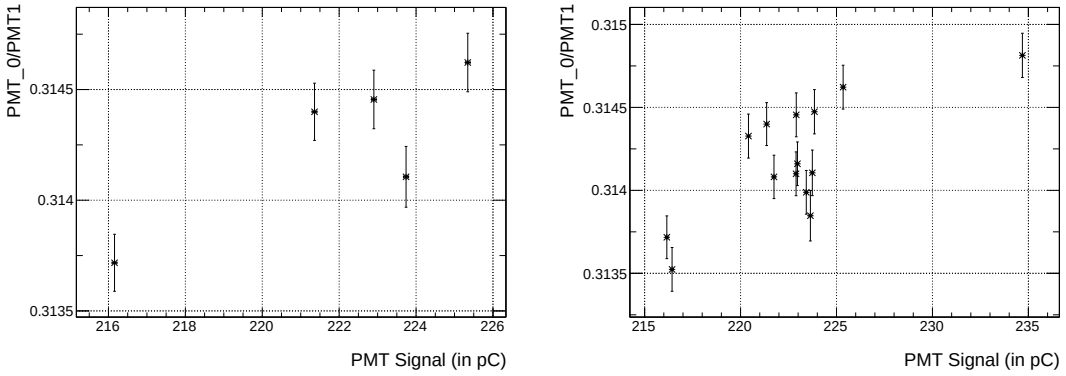

(a) 14k (b) 26k

FIGURE 5.4: Fluctuations in the Signal for the same intensity

Figure 5.4 shows the values of the ratios in the case of 14k (a) and 26k (b) intensities. There are some fluctuations in the signal not suppressed by the ratios at the low intensity that go to 4% for some PMTs and much smaller at higher intensities (<0.5%).

The impact of the variation of the temperature in the laser head on the linearity determination was also studied. Figure 5.5 shows that for a set of runs taken consecutively with intensities 14k, 26k, 14k, 26k and so on, the temperature of the laser head clearly increases with time.

The dependence of the signals in one PMT of the Tilecal (PMT_0) and in the PMT1 are shown in Figures 5.6 and 5.7 for intensities equal to 14k and 26k respectively.

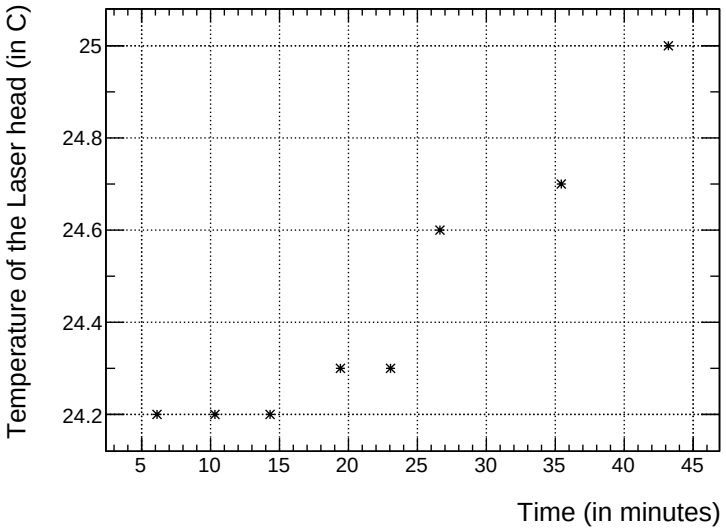

FIGURE 5.5: Temperature evolution in consecutive runs

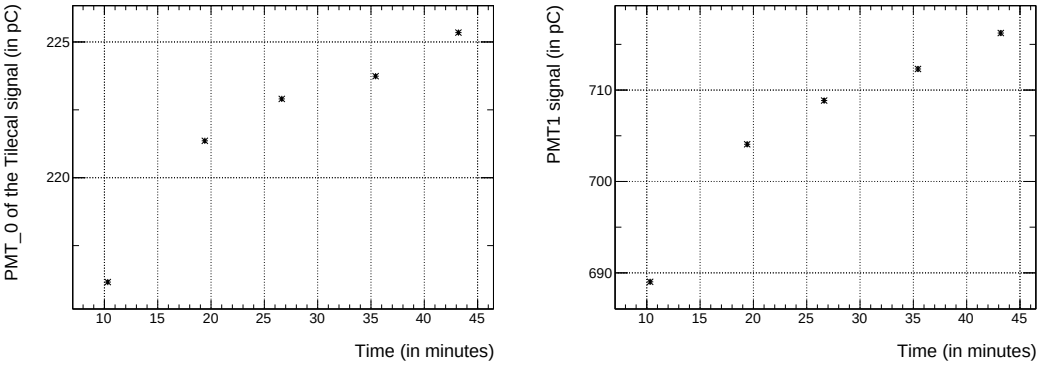

FIGURE 5.6: Signals for PMT1 and PMT_0 versus time for intensity 14k.

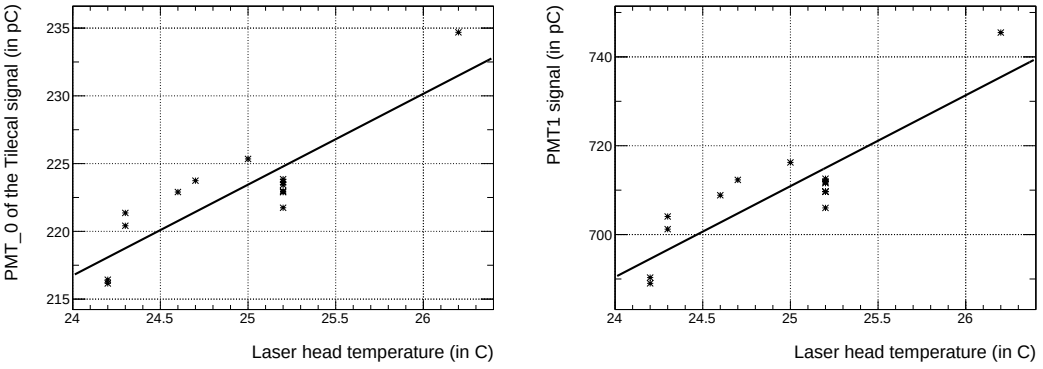

FIGURE 5.7: Signals for PMT1 and PMT_0 versus the temperature for intensity 26k, one can see there is a correlation here

For 26k it is clearly seen some correlation between the signals and the temperature. The ratios also seem correlated to the temperature (Figure 5.8). The effect is less apparent at 26k because, as shown in Figure 5.7, the change in PMT1 and PMT_0 are more correlated.

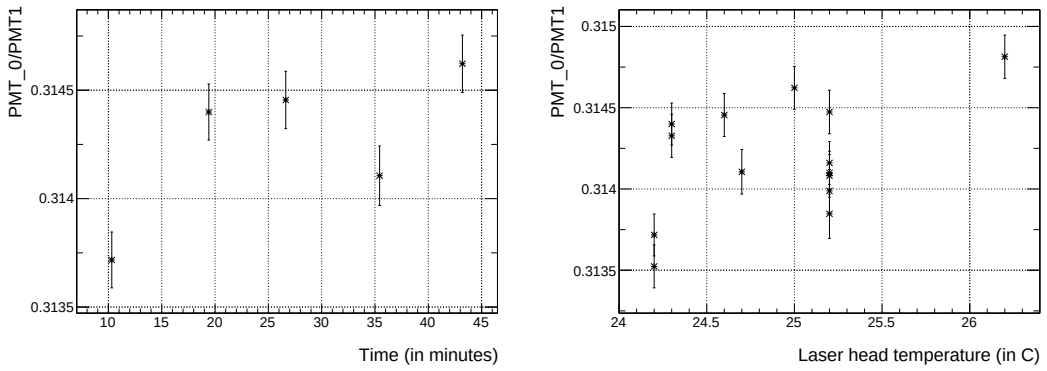

(a) 14k (b) 26k

FIGURE 5.8: Correlation between the ratios and a) time for 14k and b) the temperature for 26k

5.1.3 Different intensities with temperature

Going back to the runs analyzed at the beginning, it was compared the points with different temperatures in the Laser head.

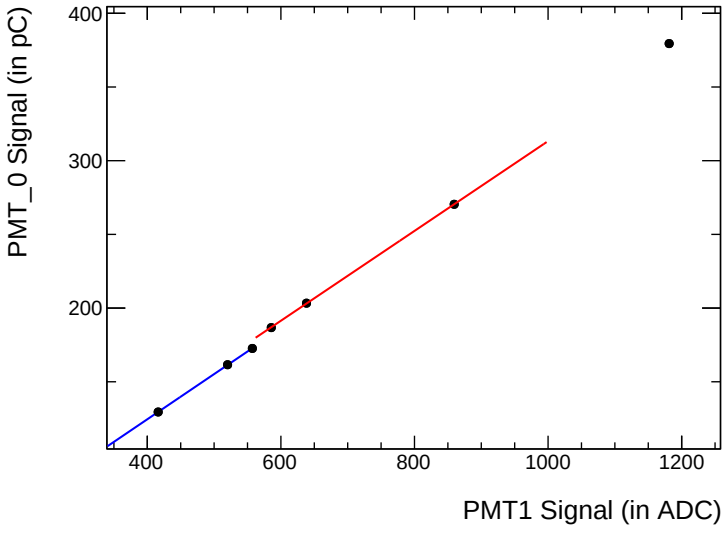

FIGURE 5.9: Linearity plot for the 1st PMT of the Tilecal

Figure 5.9 shows the scatter plot PMT_0 versus PMT1. The data shows a variation of the slope or offset around 600 ADC that seems linked to the variation in temperature

(shown in Figure 5.10). Comparing the chi-squares of the linear fit, the overall fit has χ^2/NDF=384, the blue (<600 ADC) 16 and the red (>600 ADC) 18.

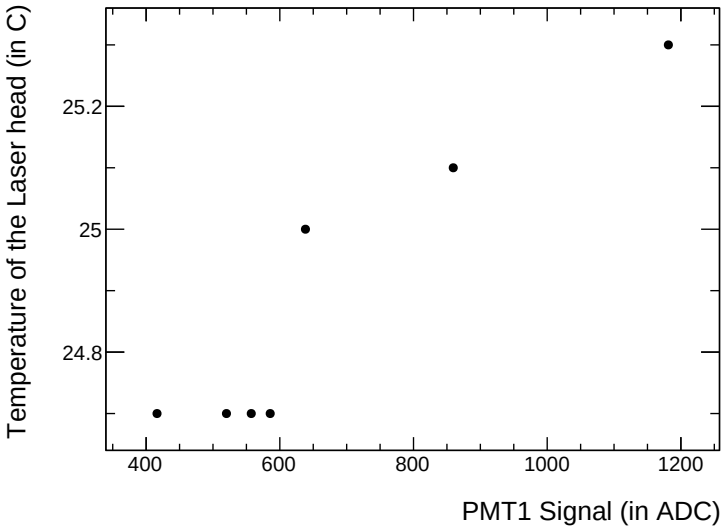

FIGURE 5.10: Change in temperature along the runs

As it is unrealistic to wait for stabilization of the LASER head temperature before taking the data, because this will take a few hours, in order to try to eliminate any kind of systematic error coming from the LASER box, one needs to use as reference a signal coming from somewhere after the laser box. There are two possibilities: use the diodes after the laser box or some PMT of the Tilecal itself. Using a PMT of TileCal as reference there could be a bias to the linearity determination because the reference device can have the same problems of the measured PMTs. They can cancel in the ratio.

5.2 Using diode 4 as reference

In order to eliminate possible effects due to temperature variation, one can use a reference after the laser box as well. One candidate are the diodes, that are expected to be not so good due to the cross-talk effect. Cutting above 1800 ADC channel, so that the saturated signals can be removed, one gets the results plotted in Figure 5.11.

Looking at the plots there is an improvement in the chi-square probability as well as the very shifted offset parameter due to the cross-talk effect. Again, there are some small bias in the residuals. But there is an improvement of the normalized residuals to 0.5%.

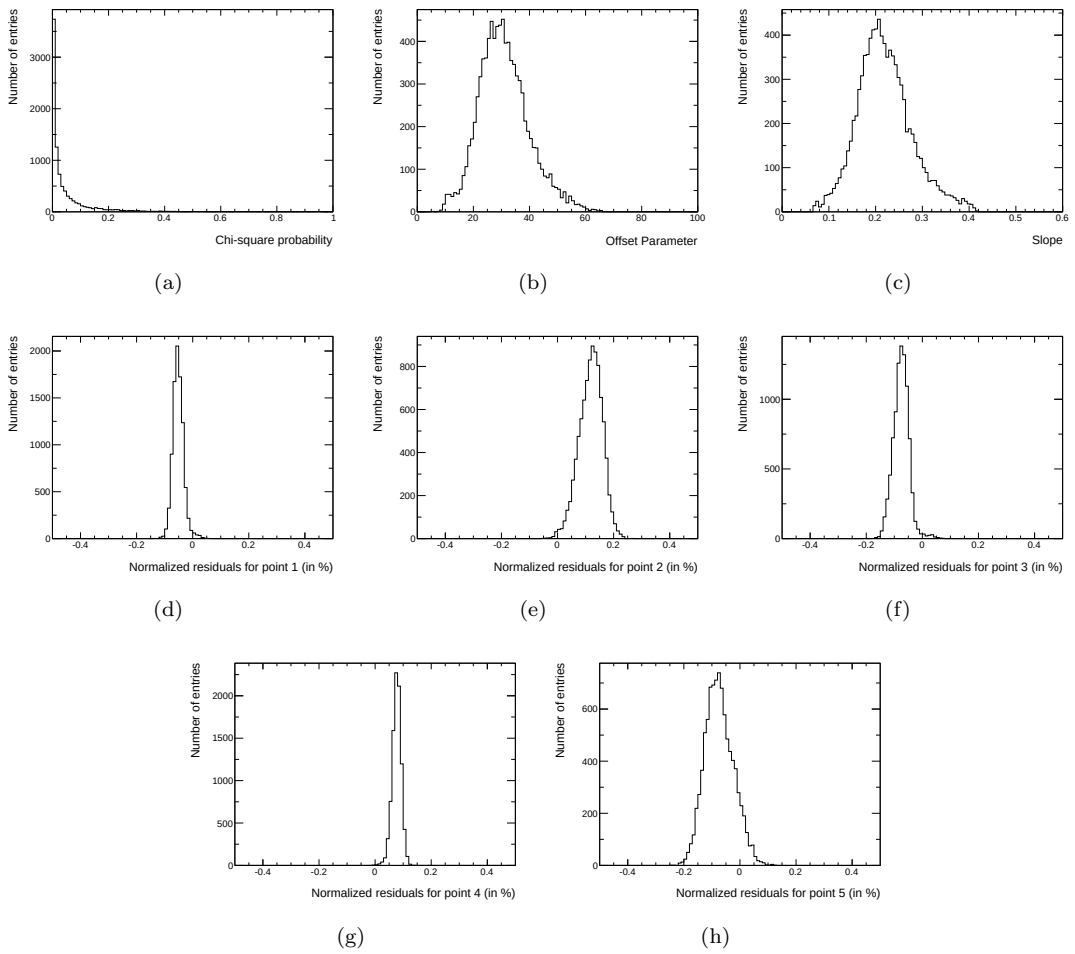

FIGURE 5.11: Histograms obtained in the study PMT vs diode 4. a) the chi-squared probability, b) the offset parameter, c) the slope, and d-h) The residuals (in %) of the points 1 to 5

5.3 Using the 1st PMT of the TileCal as reference

Using the 1st PMT of the TileCal one gets very similar results to the previous case with the obvious exception of the offset that no longer is that much shifted (no more cross-talk). Again, there are some small bias in the residuals. The results are shown in Figure 5.12.

5.4 Using the 1st PMT of the same fiber

Now, comparing only PMTs of the same fiber, one should get an improvement because they all get the same signal regardless of the effect that signal suffered being splitted in the optical apparatus. The results shown in Figure 5.13 were obtained using as reference of each PMT of TileCal the first PMT belonging to the same fiber. Indeed, when the

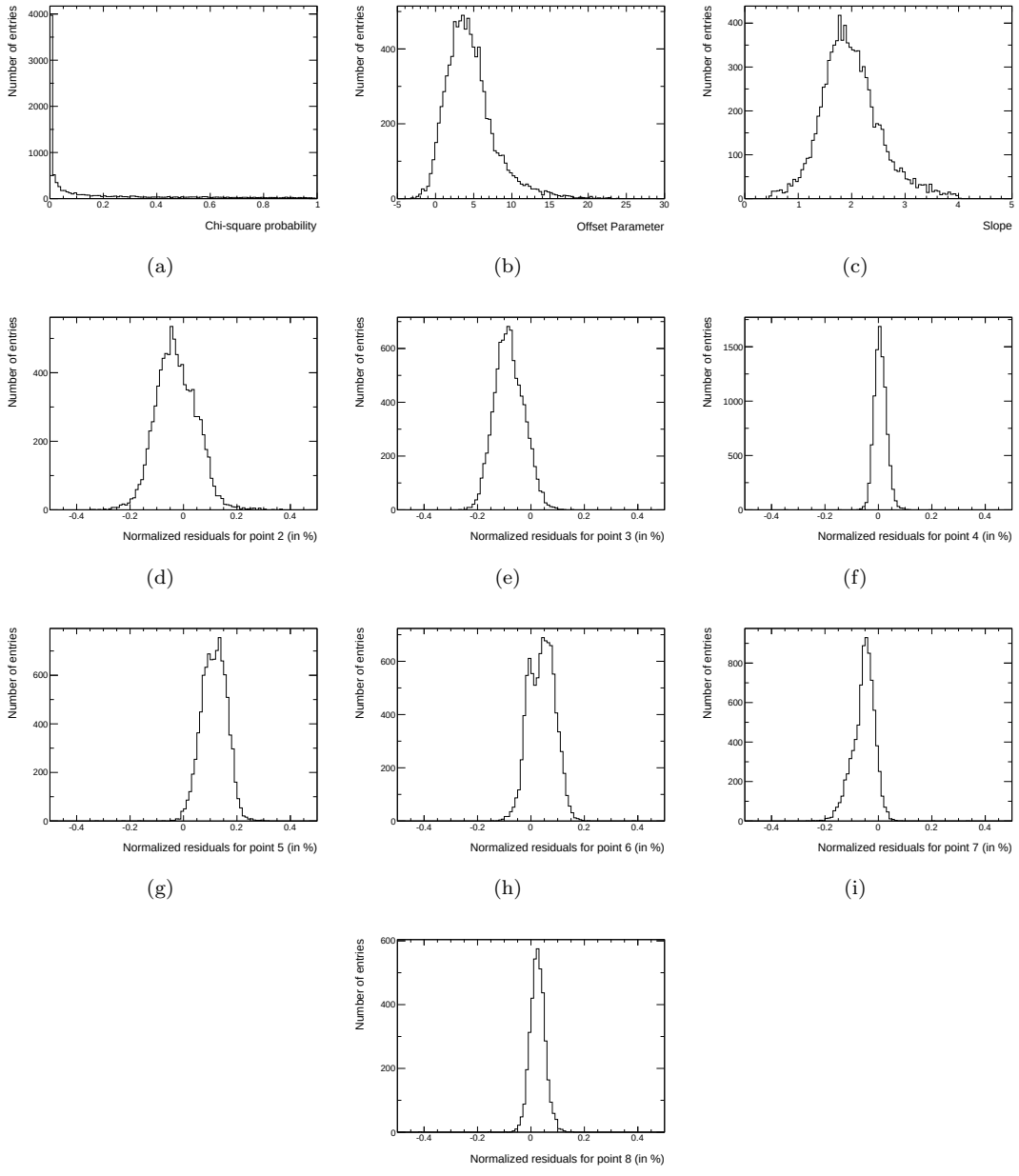

FIGURE 5.12: Histograms obtained in the study PMT vs the 1st PMT of the TileCal. a) the chi-squared probability, b) the offset parameter, c) the slope, and d-k) The residuals (in %) of the points 2 to 8

1st PMT of a fiber is used as a reference to the following PMTs in the same fiber one gets the histograms in Figure 5.13.

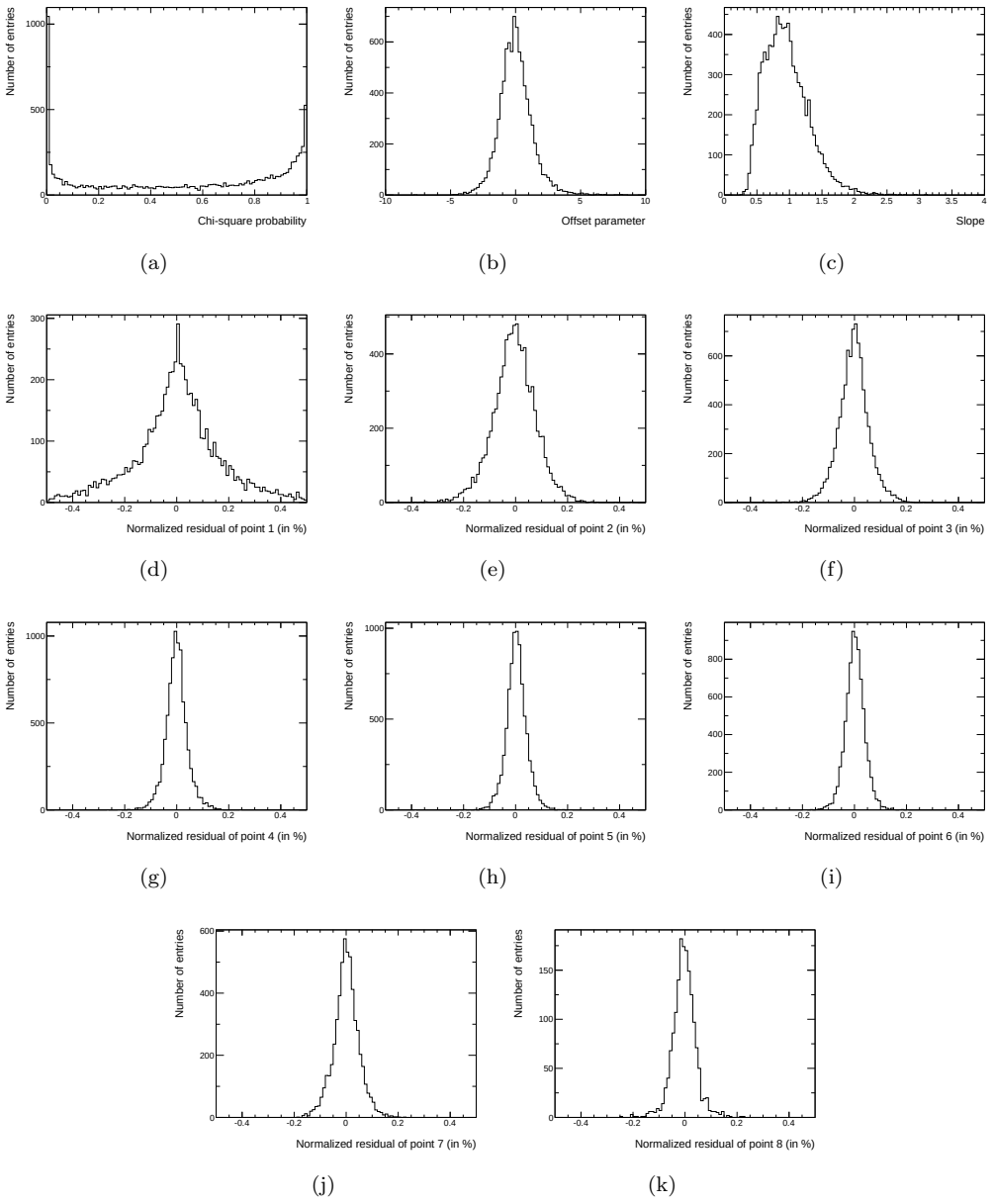

FIGURE 5.13: Histograms obtained in the study PMT vs 1st PMT of the fiber. a) the chi-squared probability, b) the offset parameter, c) the slope, and d-k) The residuals (in %) of the points 1 to 8.

As shown there is a huge improvement in the parameters. The offset is, for the first time, centered around zero, as it should be, as well as the normalized residuals. So no bias is observed using those references. One strange thing is the presence of fits with low chi-square probability. Looking at the residuals, this could be due to the 1st point that has larger values than the others. Removing that point from the fit leads to the chi-square probability shown in Figure 5.14. In this case there is a tendency (also seen

in the previous plot) of an high chi-square probability, not flat as expected. These is probably due to the fact that the PMTs of the same fibers are strongly correlated. The residuals now go to 0.2% at maximum.

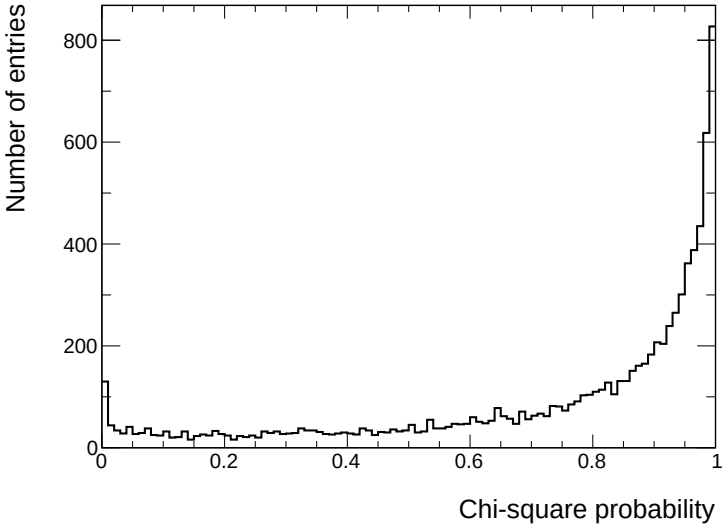

FIGURE 5.14: Chi-square probability excluding the 1st point

Chapter 6

Conclusions

It was proven difficult to quantify and describe well the various methods used in the study. This is due to the very small errors of the parameters which give always bad χ^2 probabilities. Despite that, several conclusion could be drawn.

Low intensities combined with large attenuation factors produce large residuals. As the signal is low, any small deviations from the linearity fit contribute much more than stronger intensity signals. There is also a non linearity effect in the electronics [10] that contributes to the non linearity observed and is responsible for the increased residuals.

From chapter 5 it seems there are many sources of systematic errors in the system starting from the LASER box. A change in the LASER head temperature seems to have an impact on the signal splitting produced by the splitting mirror, resulting in bad chi-squares fit probabilities and residuals that go up to 2%. Even using Diode 4 and a TileCal PMT, there are still some (small) bias in the results indicating there are also some systematics in the distribution of the light in the fibers. Regardless of this bias there is an improvement in the residuals which go up to 0.5% maximum. Those bias are finally suppressed when we look to PMTs of the same fiber. A summary of these results is shown on Table 6.1.

Method	**p0 [pC]**	**residuals [%]**	**mean of χ^2 prob distribution**
PMTs vs PMT1	∼-10	biased and <2%	0
PMTs vs diode 4	∼30	biased and <0.5%	0.05
PMTs vs 1st PMT of TileCal of TileCal	∼5	biased and <0.5%	0.16
PMTs vs 1st PMT of the same fiber	∼0	not biased and <0.2%	0.75

TABLE 6.1: Summary of the results of the various methods

Bibliography

[1] G. Aad et al. The ATLAS Experiment at the CERN Large Hadron Collider. *JINST*, 3:S08003, 2008. URL http://iopscience.iop.org/1748-0221/3/08/S08003

[2] ATLAS Collaboration. Inner Detector Technical Design Report. CERN/LHC, 97-17, 1997.

[3] ATLAS Liquid Argon Collaboration, J. Y. Hostachy. Construction and test results of the ATLAS EM barrel calorimeter and presampler. *Nucl. Phys. Proc. Suppl* 125 (2003) 112116.

[4] ATLAS Collaboration. The ATLAS Experiment at the CERN Large Hadron. *J. Instrum.*, ATL-COM-PHYS-2007-102, 2007.

[5] P.Adragna et al. The ATLAS hadronic tile calorimeter: From construction toward physics. *IEEE Trans. Nucl. Sci*, 53(2006) 1275–1281.

[6] ATLAS Collaboration. Tile Calorimeter Technical Design Report. *Tech. Rep*, CERN-LHCC-96-42.

[7] Nuno Filipe da Silva Fernandes de Castro. Study of the Wtb vertex structure at the ATLAS experiment. CERN-THESIS-2008-083.

[8] Miguel Castro Nunes Fiolhais. Study of ATLAS sensitivity to asymmetries in single top events. Master Thesis CERN-THESIS-2009-014 2008

[9] V.Garde. PHD Thesis. 2004. URL http://tel.archives-ouvertes.fr/docs/00/04/60/13/PDF/tel-00004368.pdf.

[10] D. Calvet et al. Commissioning of the ATLAS tile calorimeter LASER calibration system. ATL-COM-TILECAL-2010, May 2010.

[11] R. Alves et al. ATLAS tile calorimeter LASER calibration system. ATL-TILECAL-INT-2010-001, January 2010.